We thank the editor and reviewers for their time, and have revised the manuscript according to the comments. Our response to each comment is included in red text after each comment below. The red page and line numbers refers to the revised document.

Rewier #1

1. *Use of air temperature data in the analysis*. The authors use air temperature data recorded on the R/V Lance vessel, which appears to have been at sailing within about 100 km of the area under investigation. At this time of year the sea ice cover will be very close to its freezing point and very sensitive to slight changes in its surface energy balance, so that air temperatures recorded at some distance away may not indicate whether or not the ice is freezing or melting at the time of a SAR acquisition. While it is understandable that measurements on the ice could not be made, assertions about the freezing/melting state of the ice cover made on the basis of these air temperature readings, and how this relates to the scattering behavior and classification performance, should be made with caution. The authors should use these ancillary data to guide their analysis and discussion points. Making concluding statements on the basis of these data, however, would not be appropriate.

We agree in this point, and the treatment of the meteorological measurements in the manuscript in was improved in two ways:

1. Strong statements on the relation between the results and temperature have been balanced:

   P2L18-20: In the abstract, the last sentence was rewritten:
   "Excluding temporally inconsistent SAR features improved the segmentation in one of the X-band scenes."

   P23L12-17: In the new-written discussion-part:
   "During the week of data collection, the temperature was varying around zero degrees Celsius, introducing difficult conditions for sea ice information retrieval from SAR. The distance between the meteorological measurements retrieved from R/V Lance and the study site makes detailed analysis of SAR weather dependence difficult. Some general meteorological events observed in the meteorological data could however help explain our results."

   In the conclusion,
   P26L6-8:
   "…performed poorly. The poor performance might be a result of air temperatures above zero degrees Celsius combined with low incidence angle and polarimetric channel combination (HH-VV). Reducing the…"

   P23L11-13:
   "…,and our results indicate that an exclusion of temporally inconsistent features could improve the segmentation results in some cases. To confirm…"

2. We have included meteorological data from ECWMFs re-analysis (ERA-interim), both for the position of R/V Lance and the position of the satellite scenes. These data are included in Fig. 2, and in the following text (P9L20-29):

"…until 2 September. To investigate how the distance between R/V Lance and the position of the satellite scenes influenced the meteorological information, 2 meter air temperature and surface pressure were extracted from the European Center for Medium-Range Weather Forecastes(ECMWF) re-analysis (ERA-Interim) (Dee et al., 2011). The parameters were extracted in 6-hours increments for both the position of R/V Lance and the satellite scenes (79.25° N 14.25° W). There was good agreement between ERA-interim air temperature and surface pressure at the two locations (Fig. 2). The re-analysis seemed to overestimate the air temperature during the start of the campaign."

2. *Selection of polarimetric features*. The authors draw a connection to a previous publication in order to justify the selection of polarimetric features in this study. This seems logical, however not enough information is provided in the current paper about the expected behavior of these features for the varying system and target parameters under consideration. The authors should follow on their descriptions of the expected behaviors of Relative Kurtosis and Geometric Brightness with appropriate background information relating to the other features. While some of the target behaviors are understandably novel, expected systembased behaviors should still be provided. For example, co-polarization ratio and copolarization correlation magnitude will vary as a function of incidence angle across the 10° range between R1 and R2. Variations in the co-polarization correlation magnitude between R1, R2, and R3 do appear to trace the variations in incidence angle, at least for ROIS 1-4, which somewhat contradicts the assertion made in lines 5-10 on page 4554.

To meet this request, we have added brief background information about all investigated features in the method section, P12-13L22-9:
"…smaller eigenvalues. $R_{VH/VV}$ is known as a measure of depolarization (Drinkwater et al., 1992). In microwave scattering of sea ice, depolarization is expected related to multiple scattering within the sea ice volume or to surface roughness (Scharien et al., 2012, Moen et al., 2013). $R_{VV/HH}$ is only dependent on the relative permittivity for very smooth surfaces within the Brag regime (Hajnsek et al., 2003). For rougher surfaces, the feature is expected to increase with incidence angle and relative permittivity, and decrease with increasing surface roughness (Drinkwater et al., 1991, Fung, 1994). With volume scattering, $R_{VV/HH}$ (dB) tends toward zero (Scharien et al., 2012). $|\rho|$ is a measure of the proportion of polarised backscatter, reaching unity when the co-polarisation channels are perfectly correlated (Drinkwater et al., 1992). The feature is expected to decrease with incidence angle, at an increasing rate for high salinity ice (Drinkwater et al., 1992, Gill et al., 2012). $<\rho$ is the relative difference in phase between the co-polarisation channels, describing the sea ice scattering history (Drinkwater et al., 1992). The feature depends on both the sea ice relative permittivity and surface roughness."

Hajnsek et al., 2003, Drinkwater et al., 1991 and Gill et al., 2012 were added to the reference list.

We have reconsidered the assertions made in lines 5-10 on page 4554, and this part of the manuscript was reformulated (P22L6-13):
"The incidence angle of the three RS-2 scenes varies between 38 and 48 degrees (see Table 1). $|\rho|$ varies linearly with incidence angle, according to Fig. 6, the same dependency cannot be seen for $R_{VV/HH}$."

The same topic has been commented on in the new-written discussion part (P22-23L29-1):

“From Fig. 6, it seems like the influence of the changing incidence angle is limited, except for |ρ|.”

3. *Classification versus segmentation*. The term “segmentation” is used extensively, including the title. Segmentation typically refers to dividing an image into groups of connected pixels. What is being done here is an image classification, the labelling of pixels.

We agree that the term segmentation may need further explanation, and we used this term deliberately to distinguish it from the term classification. Classification commonly brings with it the understanding that you know what the "classes" represent. Although our segmentation algorithm (essentially a clustering algorithm) assigns a numeric label to each pixel, the value is a randomly chosen index for each group (cluster) holding no identification information (apart from that those pixels with the same label have similar statistical properties). This type of image segmentation is somewhere between a contiguous (connected) domain based segmentation, that the reviewer mentions, and an image classification to known classes. We have not found a better term to really convey this distinction.
Our work is a first step towards developing a true classification, where we now have to identify the uninformative labelled segments to assign meaningful class labels (i.e., ice types). Moen et al (2013) also used the term segmentation, and we think this term gives the most accurate description of our algorithm.

To make this clearer in the text, we made the following changes:

P2L15-18: The sentence was rewritten and expanded
“In C-band, the algorithm produced a good late summer sea ice segmentation, separating the scenes into segments that could be associated with different sea ice types in the next step. The X-band performance was slightly poorer.”

P5L19-21: An extra sentence was added
“Secondly, the feature-based automatic segmentation algorithm is tested on our dataset. We investigate whether it groups the scenes into reasonable segments, possible to associate with distinct sea ice types. The algorithm….”

P14L22-26: The sentence was rewritten
“The algorithm was set to segment the scenes into six different segments. The number was chosen to allow for the five sea ice types described by the ROIs, in addition to one extra segment to allow for detection of other sea ice types and to assure some flexibility for the algorithm.”

P14-15L28-2: was rewritten
“For each scene, the segmentation's performance is evaluated visually on its ability to separate the four main sea ice types represented in the ROIs (medium thick FYI, thin FYI, old ice and old deformed ice), and based on its ability to discriminate the pixels of the five ROIs into different segments.”

P20L9: The sentence was rewritten
“Figure 9 displays which segments the pixels of each of the ROIs were assigned to…”

P21L7-8: The term “classes” was changed to “segments”
“Figure 11 displays which segments the pixels in each of the ROIs are assigned to in the segmentation of the two TS-X scenes.”

P24L14: The term classes was changed to “segments”
“…size and number of segments are important…”

P24L23-29: The term class(es) was changed to “segment(s)”
“The number of segments was set in advance, based on visual inspection of the scenes and information retrieved from the helicopter-borne measurements. Choosing too few segments could force different ice types into a common segment, while increasing the number of segments could split an ice type into several segments.”

P26L22-26:
“Future studies should also focus on a better physical understanding of the relation between SAR polarimetric features and geophysical properties. This could improve the interpretation of the segmented sea ice scenes, and possibly lead to an automatically labeling the segments, a classification.”

Caption Fig. 8: The term classes was changed to segments
“Segmentations of the three Radarsat-2 scenes (R1, R2 and R3) into six segments.”

Caption Fig. 9: The term classes was changed to segments
“The segments assigned to the pixels in the five regions of interest by…”

Caption Fig. 10: The term classes was changed to segments
“Segmentations of the two TerraSAR-X scenes (T1 and T2) into six segments.”

Caption Fig. 11: The term classes was changed to segments
“The segments assigned to the pixels in the five regions of interest by”

4. *Organization and writing*. The results section includes long descriptions of methods and justifications for investigations that were either previously provided or belong elsewhere. For example see beginning of Section 3.13:the background information on sea ice permittivity is important, but would make sense if it were provided much earlier. As it is, the results section is cumbersome to read. It should be edited so that focus is on key results and discussion points. The paper should also be edited to make sure the correct tense is being used consistently (e.g. line 10 on page 4547, “(ROIs) were chosen” etc.).

We thank the reviewer for this opportunity to reconsider the results and discussion section. We have gone through the section with the reviewers comments in mind, and restructured it. In this work, we divided the section into a result and a discussion part. The use of tense was also edited. See the revised document for changes.

Tense was also changed in the following sentences in the method section:
P6L1: “…,five regions of interest (ROIs) with different sea ice types were defined…”

P6L14-16:“The study site was situated in this area (Fig. 1). Both FYI and old sea ice in different stages of development were represented at the site”

P10L4-6:“The area covered by the satellite scenes consisted of sea ice with different geophysical properties. Some regions were homogeneous and some contained mixtures of different sea ice types.”

P10L18:“ROI1 represents an area…”

P10L19:“The sea ice in ROI1 was relatively smooth and had a moderate melt pond fraction.”

P10L21:“The sea ice in ROI2 was smooth…”

P11L6:“The features studied were previously…”

P13L18:“The probability density functions (PDFs) were estimated”

P13L22-25:“As the ROIs investigated were small, resulting in small sample sizes, leave-one-out cross validation was used in training and testing the classifier. A 7x7 pixels neighbourhood, L=49, was used…”

P14L1: “each individual feature were used”

P14L26-27:“segmentation was confined”

5. *Sea ice in the Fram Strait*. More background information on sea ice conditions characteristic of the Fram Strait would significantly improve the quality of the paper. It would also make it easier for readers not familiar with the ice conditions in that region to assess the potential utility of the classification approach or individual polarimetric features for sea ice detection and discrimination studies elsewhere.
To meet this request, we have added a section about the Framstrait in the Method section (P6L5-16):

2.1 Study site
Fram Strait is a dynamic region characterised by the outflow of sea ice from the central Arctic Ocean (e.g. Kwok, 2009b, Renner et al., 2014). The sea ice cover is therefore highly variable with both multiyear and first-year ice, and contains a large fraction of deformed ice. In late summer, the snow cover has usually melted completely, leading to melt ponds on top of the ice (e.g. Renner et al., 2013). While in most parts of Fram Strait, southward drift leads to fast movement of the sea ice, a region with iceberg-fast ice forms in some years in western Fram Strait (Hughes et al., 2011). In this region, the ice cover varies between rough ice due to deformation and very level ice where the ice is formed during winter and protected from impact (Beckers et al., 2015; unpublished data). The study site was situated in this area (Fig. 1). Both first-year sea ice (FYI) and old sea ice in different stages of development were represented at the site.

Hughes et al. (2011) and Kwok (2009b) was added to the reference list.

P7L1-3 was removed.

Technical corrections:
P=Page, L=Line
P4540L6: These remotely sensed data are not *in situ*.
P2L6: The term "In situ" was removed
"Sea ice thickness, surface roughness and aerial photographs were collected during a helicopter flight at the site."

P4540L9: 'temporal'
P2L12: The misspelling was corrected.

P4541L7: give the dual polarization combination used by ice services (HH + HV or VH + VV)
P3L8 and P3L11: The combinations were added
"…dual polarimetric SAR images (HH + HV or VH + VV) in sea ice monitoring…"
"…full polarimetric SAR imagery (HH + HV + VV)."

P4541L8: swath 'widths'
P3L9: The misspelling was corrected.

P3L15: State the C-band frequency in GHz, as done below for X-band.
P3L41: The frequency was added
"C-band (5.4 GHz) is considered…"

P4541L16: 'to investigate' instead of 'in investigating'.
P3L17-18: The wording was changed
"…new opportunities to investigate the potential…"

P4541L19: 'platforms'
P3L21: The misspelling was corrected.

P4542L9: 'derived from' instead of 'based on'
P4L66: The sentence was rephrased.

P4542L20-27: This could be split up into two sentences to improve readability.
P4-5L12: The sentence was split up and rephrased:
"Newer studies include examination of backscatter signatures of multiyear sea ice with ship-based scatterometer (Isleifson et al., 2009) and investigation of the use of a supplementary frequency of either X- or Ku-band in addition to C-band in late summer sea ice classification with an airborne scatterometer (Brath et al., 2013). Satellite based studies include separation of MYI and FYI by dual polarisation intensity from Radarsat-2 (Warner et al., 2013), classification potential of polarimetric features from Radarsat-2 (Gill et al., 2013) and investigations of melt

pond fraction retrieval from co-polarisation ratio data acquired by Radarsat-2 (Scharien et al., 2012, 2014b)."

P4543L10: 'individual'
P5L16: The misspelling was corrected.

P4543L24: delete 'detailed'
P6L4: "detailed" was removed.

P4544L2: '… ship, helicopter, and satellite platforms…'
P6L18: "platforms" was added.

P4544L6: '…from the scientific vessel R/V Lance provided information …' (delete 'are also available')
P6L22: The sentence was rephrased.

P4544L9: delete 'ground based'
P6L25: "Ground based" was deleted.

P4544L18: '… and the positions…'
P7L8: The misspelling was corrected.

P4544L19: ' … scenes were acquired during ascending orbits.'
P7L9: The sentence was rephrased.

P4544L22: 'Air- and ship-borne measurements' or 'Airborne and shipborne measurements'
P7L11: The title is rephrased to "Airborne measurements", and the following subtitles "Sea ice thickness", "Surface roughness" and "Melt pond fraction" were removed .

P4545L8: 'From this device …'
P7L22: The sentence was rephrased.

P4545L13: How is it known that there is very little or no snow cover? More detail is needed to back up this observation.
Information about the snow cover is retrieved from the downward-looking helicopter photos and from scientists onboard the helicopter. The sentence was expanded (P8L2-3):
"At the time of the acquisition there was very little or no snow on top of the sea ice, confirmed by the aerial photos and observations from scientists onboard the helicopter."

P4546L5-18: How reliable are the classified images? Was an accuracy assessment performed?
An accuracy assessment was performed by Renner et al. (2013). A sentence was added to specify this (P8L21-22):
"as described in Pedersen et al. (2009) and Renner et al. (2013). In an accuracy assessment of the method performed in Renner et al. (2013), 76 % of the melt pond pixels were correctly classified."

P4546L22: Provide information regarding the meteorological instrumentation and measurement

height.
The height of the automatic weather station was about 22 above sea level. The instruments consist of an air temperature sensor 3455, an air pressure sensor 2810 and a relative humidity sensor 3445, all from Aanderaa data instruments. This information was included in the manuscript:

P9L12-15: The sentence was expanded
"An automatic weather station at R/V Lance consisting of an air temperature sensor (3455), an air pressure sensor (2810) and a relative humidity sensor (3445), all from Aanderaa, were recording metorological information during the campaign (Fig. 2). The height of the station was 22 meters above sea level."

P4547L10: '…(ROIs) were chosen …'
P10L8: The misspelling was corrected.

P4547L19: It would be more appropriate to indicate that the ice types were labelled according the WMO sea ice nomenclature, in addition to providing the reference.
P10L15-17: The sentence was rephrased
"Table 2 presents helicopter measurements for each ROI, including mean and modal sea ice thickness, mean melt pond fraction, surface roughness, and sea ice class labels according to WMO sea ice nomenclature (World Meteorological Organisation, 1989)."

P4547L23-25: '…is smooth with a high melt pond …' ; 'ROI3 and ROI4 represent areas of weathered and deformed old ice …' ; 'ROI3 represents thinner ice with a higher melt …'
P10L21-23: The sentences were changed.

P4548L4: delete different
P11L2: "different" was deleted.

P4548L6: Sentence 'This study investigates … ' should be deleted (stated already).
P11L4-5: The sentence was deleted.

P4548L18: 'Assuming reciprocity …'
P11L16: The misspelling was corrected.

P4550L5: 'Bayes' decision rule'
P13L14: The misspelling was corrected.

P4550L12: delete hence
P13L23: "Hence" was deleted.

P4551L1: pdf should be PDF
P4552L21: PDF
P13L18 and P16L11 pdf was changed to capital letters.

P4552L26: '… is not necessarily a result…'
P16L16: The misspelling was corrected.

P4553L4-5: '…evolution of feature means from each ROI are displayed in …'
P16L23-24: The sentence was corrected.

P4553L13: '…searching for temporally consistent'
P17L6: The misspelling was corrected.

P4554L3-9: Did you try subtracting the additive noise from the RS-2 scenes before calculating RVV/HH? These data are found in the RS-2 header files. This method has been shown to improve
RVV/HH estimates of ocean and ice at the high incidences analyzed here.
We did not try to subtract the additive noise in this study, but will keep it in mind in future investigations.

P4554L10-15: Did Gill et al. (2013) look at the late summer period? Please clarify.
The study of Gill et al. was performed in late winter/spring, as stated in P4554L10. The study was mentioned as it investigated polarimetric features temporal consistency when temperatures were varying from below to zero degrees Celsius. The last sentence in the paragraph was changed to emphasise that the season was different in their and our study (P22L13-19):
"The differences in results may be explained by different incidence angles, sea ice types, snow conditions and season."

P4555L8: '…could solely discriminate all ROIs…' (delete 'between')
The sentence was removed in the rewritten results section.

P4556L5: '…helicopter flight…'
P19L21: The misspelling was corrected.

P4556L14: '… scenes are small.' (delete 'in general')
P20L7: "in general" was deleted.

P4556L18: '… with the full feature set give …'
P20L11: The misspelling was corrected.

P4557L3-4: Here the parameters are given in text form when the symbols were previously given. Best to stick with using the symbols.
This part of the sentence was removed in the rewritten results section.

P4557L13-15: This sentence should be re-written for clarity. The rest is very well described.
The sentence was changed to (P21L7-9):
"Figure 11 displays which segments the pixels in each of the ROIs are assigned to in the segmentation of the two TS-X scenes. For T1 both for the full achievable (left) and the reduced (right) feature set."

P4558L3: 'acquisition'
P24L6: The misspelling was corrected.

P4558L5-6: As given it is not clear how both of these processes (formation of rime, refreezing of

the ice) would lead to a lower contrast between sea ice types. The occurrence of either is plausible and worthy of mention, as per the conditions. However the authors should be cautious attributing these processes to reduced ice type discrimination. Could a refreezing of the sea ice lead to increased microwave penetration depth and enhanced ice type discrimination on the basis of volume scattering differences between ice types?
This is an important aspect to bring in, and the sentence was rephrased to include it (P24L9-12): "Both of which could cause a lower contrast between different sea ice types, and hence hamper the segmentation results. A refreeze of the sea ice could however also possibly result in the opposite, enhanced volume scattering could lead to increased sea ice type discrimination."

P4558L20: add a period to the end of the sentence
The sentence was rewritten in the new discussion part.

P4558L24: '… at the time of acquisitions could all contribute to poorer segmentations.'
The sentence was rewritten in the new discussion part.

P4559L3: *in situ* data were not used
This is very correct, the term "in situ" was removed and the sentence rewritten (P24L23-25): "The number of segments was set in advance, based on visual inspection of the scenes and information retrieved from the helicopter-borne measurements."

P4559L24: Another possible reason would be a higher sensitivity to incidence angle.
We agree in this, and changed the sentence to (P25L18-20):
"Possible reasons for the two features inconsistency could be a higher sensitivity to changes in relative permittivity or incidence angles."

P4560L4: '… evaluated visually for its ability …'
The sentence was changed to (L25P25-26):
"…and evaluated for its ability to…"

P4560L6-7: 'The segmentation in general performed well …'
P25-26L28-29: The sentence was changed.

P4560L16: 'temporally'
P26L12: The misspelling was corrected.

Figure 9 caption: 'assigned'
Figure 11 caption: 'assigned'
The misspellings were corrected.

Reviwer #2

Specific comments and technical corrections:

P4541L22-25: A slightly contrasting claims in two subsequent sentences. First, "… C- and X-band ..
largely equivalent", then "X-band … add information when used .. with C-band".
C: It seems that this issue is still open. Reformulate the sentences.
P3L24-28: We agree in this, and the sentences was reformulated
"Results from the Baltic Sea suggest that the information content in C- and X-band are largely equivalent (Mäkynen and Hallikainen, 2004; Eriksson et al., 2010), while X-band was found to add information when used in combination with C-band in the Arctic Ocean (Brath et al., 2013)."

P4543L10: Individual
P4544 L8: opportunity
P5L14 and P6L24 The misspellings were corrected.

P4545L12: The footprint of the EM-bird has a diameter of about 50 m.
General question (not related only to the EM measurements):
Please add in the text your opinion about the scales in which SAR image is geophysically reasonable to analyze. For which purposes, except for scientific research, sea ice type classifications in resolutions from 10 m to 100 m are needed? (Leads, heat budget, …).
We find the question two-folded.
1.The input scale or resolution of the segmented scene govern what kind of information you can get out. Information about structures like ridges, melt ponds and small leads all require a high resolution, while general sea ice type segmentation possibly could be performed on scenes with lower resolution.
2.When it comes to the required output resolution, this depends on the application. Climate scientist are often interested in large areas, while high resolution information is needed for instance for ship navigation or structures like oil platforms.

To comment this in the text, the following sentences were added to the new discussion part (P24L18-23):
"The choice of window size will also determine which kind of information one can retrieve about the sea ice surface. If information about small-scale structure like ridges, melt ponds and small leads are important, this requires a small window. For more general information for instance about sea ice age, larger window sizes could be more appropriate. Choice of sensor would set restrictions on how high resolution it is possible to achieve, and high resolution is at the moment coupled to small swath width."

P4549L7: dual-polarimetric
P12L5: The misspelling was corrected.

P4549L10: 'G'
C: Did you mean B or where is G defined?
P12L8: This was supposed to be B, and was corrected.

P4550L5: ‘supervised classifier’
C: An essential part of the supervised classification is the selection of the training areas. Here this question is ignored. How were the classwise training areas selected, how large were they? Were they selected just from one SAR scene (a good choice) or from several scenes? In the latter case the temporal evolution of the features has been implicitly included. Hence, the classification results are not as representative as in the former case.
The MAP supervised classifier was used scene-wise to evaluate the individual features discrimination capability, and was not a part of the segmentation algorithm (which is described in P4550L25-P4551L15). The training areas corresponds to the pixels in the ROIs, described in section 2.2.1. The evaluation was done scene-wise, using leave-one-out cross validation for training. To clarify this, the following sentence has been added (P13L21-22):
“…in Bowman and Azzalini (1997). The pixels in the five ROIs were used as training areas, and each the satellite scenes were classified individually.”

The scene-wise procedure has also been stressed (P13-14L26-2):
“The resulting classification accuracies obtained for each individual feature are used to evaluate the discrimination abilities of the features in each of the five scenes.”

P4550L14-16: A 7×7 pixels neighbourhood, $L = 49$, is used in the classification and a stepping window with steps of 5×5 pixels was employed to reduce neighbourhood overlap.
C: Do you have used the same resolution for RS-2 and TSX imagery? If not, then why not? The variation of ice surface roughness and other ice features on sea ice layer remain the same independent of the resolution of the sensor. So it would be logical to analyze them in the same resolution, especially if one wishes to compare two different frequencies.
In the manuscript, we chose to use the same neighbourhood/filter size for all scenes, even if the resolution of the scenes were different. This was done from a statistical point of view, we wanted equal sample sizes. Especially the statistical feature, RK, was expected to depend strongly on sample size. However, in the work with the manuscript we did try to regulate the filter size after the resolution of the scenes as the reviewer suggest, applying different filter sizes for each scene. We experienced that choosing the filter size the one way or the other did not affect the results to a noticeable degree.

To clarify our choice for the readers of the manuscript, the following sentence was added to the manuscript (P14L20-22):
“…granular segmentations. The size of the neighbourhood does not take into account the difference in resolution between the scenes, but assure an equal sample size in the extraction of the features.”

The question was also discussed in the new-written discussion-section (P23L5-11):
“To gain equal sample sizes in our study, the same neighbourhood size was used in filtering all scenes even if the scenes resolution differed. The scenes with highest resolution would therefore have smaller filter sizes in meters. This difference in scale possibly influences the signature of physical properties of the surface, like surface roughness variation. We did, however, during our investigations, also try to use filter sizes adjusted to the resolution, but this made little difference to the results.”

P4552L1 ‘ segmentation uses ..’
C: Do you utilize here a six-dimensional pdf or 6 independent one –dimensional pdfs? If the former option, how do form a 6-D nonparametric density function? Clarify text.
The Gaussian mixture modelling is parametric. It uses a 6-D multivariate Gaussian distribution, parameterised by a mean vector and a covariance matrix, per model. To clarify this in the text, multivariate was added to the sentence (P14L12):
“The segmentation uses multivariate Gaussian mixture models to model the features' PDF, and employs an expectation-maximization algorithm.”

P4551L7-9: A stepping window with steps of 5×5 pixels was used to reduce neighbourhood overlap, and an additional sub stepping window of 10× 10 pixels was used during the algorithm for computation efficiency.
C: This sentence is an unnecessary computational detail. Remove.
P14L18-20: We agree in this, and the sentence was removed.

P4551L10-11: The algorithm was set to segment the scenes into six different classes, to allow for detection of the major sea ice types visually expected to be present in the scenes.
C: Write out the selected ice classes. Assign also to each color in Figs. 8 and 10 the corresponding ice class, like in Fig. 4 in Moen et al. (2013). It is difficult for the reader to assess the images when the color label explanations are imbedded in the text.
This question add to the classification/segmentation confusion discussed under point 3 in the reply to reviewer #1.

P14L22-26: To specify which sea ice types we have in mind, the sentence was changed to:
“The algorithm was set to segment the scenes into six different segments. The number was chosen to allow for the five sea ice types described by the ROIs, in addition to one extra segment to allow for detection of other sea ice types and to assure some flexibility for the algorithm.”

Fig. 4 in Moen et al. (2013) presents images classified by sea ice scientists, while Figs. 8 and 10 in our manuscript present segmentations, not classified images. With information from only one single flight-line through the scenes, we don’t think it is appropriate to label all segments in segmented images. We have however tried to give similar positioned segments similar colors in all five scenes, to ease the access for the reader. In the revised results-section (see reply to reviewer #1), the parts describing the segmentation results have been rewritten for easier access.

P4552L8: ‘received’
This word was removed in the revised result section.

P4554L1: Differences in … resolution could also cause the lower accuracies in the X-band scenes.
C: Do you mean that a finer resolution is a disadvantage? You can always decrease the resolution.
Please clarify.
We agree that this part of the sentence is confusing. The resolution term is brought in due to the differences in scale, as already commented on by the reviewer. We have rephrased the sentence, removing the resolution part (P16L19-20):

"…information. The lower incidence angles of the TS-X scenes could also contribute to the observed differences."

The issue of different scales is commented on in the new-written discussion part (see reply to reviewer #1).

P4556L1-15 and P4557L1-12: You can remove the references to the colors when you have added the color labels in Figs. 8 and 10 (see an earlier comment). This also improves the clarity of the text.
P4556-4557: I would prefer using the class labels in Section 3.2. instead of the ROI abbreviation. Then it would be easier for the reader to follow the text.
We refer to answer about class labeling in earlier comment.

P4558L12-20: '…The meteorological conditions could explain the poor segmentation of T1….'
C: It is worth noting that R2 was acquired just 24 hours later than T1. Around R/V Lance the air temperatures remained during this period close to zero degree Celsius. However, the results for R2 were good unlike for T1. In this case C-band SAR scene was more informative than X-band scene although the weather conditions were likely very similar for T1 and R2.
Add a sentence or two about this in the text.
We agree in this, and have reformulated the sentence, and the following paragraph to account for this. The text is included in the new-written discussion section (P23-24L17-5):
"Both T1 and R2 were acquired during a period with air temperatures close to or above zero degrees Celsius, conditions which is on the limit of suitable for sea ice type discrimination by SAR. As reported by (Scharien et al., 2010), moisture in the upper sea ice layer could mask out volume scattering and hence lower the backscatter contrast between different sea ice types. The difficult conditions could explain the poor segmentation performance of T1. However, R2 was acquired during similar meteorological conditions with good segmentation results. Lower frequency, higher incidence angle and extra information contained in the cross-pol channel (lacking for T1) could all have contributed to a better segmentation of R2."

P4560L11-13: In the other scene the segmentation performed
poorly, probably due to air temperatures above freezing point and hence difficult conditions for sea ice characterization by SAR.
C: The classification results were poor for X-band SAR (T1) but not for C-band SAR (R2). Reformulate text.
The text was reformulated (P26L6-8):
"… poorly. The poor performance might be a result of air temperatures above zero degrees Celsius combined with low incidence angle and polarimetric channel combination (HH-VV)."

P4569. Table 4 text: The best result for each ROI and the best overall accuracy for each scene are highlighted in bold.
C: Where is the best overall accuracy? I can not see that in Table 4.
This was a misprint. The sentence is corrected to:
"The best result for each ROI in each scene is highlighted in bold."

Manuscript prepared for The Cryosphere Discuss.
with version 2015/04/24 7.83 Copernicus papers of the LaTeX class copernicus.cls.
Date: 18 December 2015

Late summer sea ice segmentation with multi-polarisation SAR features in C- and X-band

A. S. Fors[1], C. Brekke[1], A. P. Doulgeris[1], T. Eltoft[1], A. H. H. Renner[2], and S. Gerland[3]

[1]Department of Physics and Technology, University of Tromsø – The Arctic University of Norway, 9037 Tromsø, Norway
[2]Institute of Marine Research, 9294 Tromsø, Norway
[3]Norwegian Polar Institute, FRAM Centre, 9296 Tromsø, Norway

Correspondence to: A. S. Fors (ane.s.fors@uit.no)

Abstract

In this study we investigate the potential of sea ice segmentation by C- and X-band multi-polarisation synthetic aperture radar (SAR) features during late summer. Five high-resolution satellite SAR scenes were recorded in the Fram Strait covering iceberg-fast first-year and old sea ice during a week with air temperatures varying around zero degrees Celsius. ~~In situ data consisting of sea~~ Sea ice thickness, surface roughness and aerial photographs were collected during a helicopter flight at the site. Six polarimetric SAR features were extracted for each of the scenes. The ability of the individual SAR features to discriminate between sea ice types and their temporally consistency were examined. All SAR features were found to add value to sea ice type discrimination. Relative kurtosis, geometric brightness, cross-polarisation ratio and co-polarisation correlation angle were found to be ~~temporally~~ temporal consistent in the investigated period, while co-polarisation ratio and co-polarisation correlation magnitude were found to be temporally inconsistent. An automatic feature-based segmentation algorithm was tested both for a full SAR feature set, and for a reduced SAR feature set limited to temporally consistent features. In ~~general~~C-band, the algorithm ~~produces~~ produced a good late summer sea ice segmentation~~.~~, separating the scenes into segments that could be associated with different sea ice types in the next step. The X-band performance was slightly poorer. Excluding temporally inconsistent SAR features improved the segmentation ~~at air temperatures above zero degrees Celcius~~in one of the X-band scenes.

1 Introduction

A decline in the Arctic sea ice extent has been observed during the last decades, together with a large reduction in sea ice thickness and sea ice volume (Kwok et al., 2009a; Parkinson and Comiso, 2013; Laxon et al., 2013; Meier et al., 2014). The reduction in sea ice volume has also lengthened the melt season at a rate of about five days per decade since 1979 (Stroeve et al., 2014). To understand the processes governing these changes, and

to meet the needs of shipping, oil and gas industries in an increasingly accessible Arctic, more detailed mapping and monitoring of the summer sea ice cover is required (Stephenson et al., 2013).

Synthetic aperture radar (SAR) is widely used in operational sea ice monitoring. The Canadian Ice Service alone processes ten to twelve thousand SAR images every year (Moen et al., 2013). Operating in the microwave frequency, SAR has the advantage of providing all-weather and day-night imagery. At present, operational sea ice services use single and dual polarimetric SAR images (HH + HV or VH + VV) in sea ice monitoring due to their wide swath ~~width~~ widthS and good temporal coverage. However, on a local scale, more information and improved sea ice segmentation can be retrieved from full polarimetric SAR imagery (HH + HV or VH + VV). Today, such data is in limited use mainly due to its reduced coverage. The recent development of compact polarimetry could open the way for more polarimetric radar information to be retrieved at larger swath widths (Raney, 2007; Dabboor and Geldsetzer, 2014).

C-band (5.4 GHz) is considered the preferred frequency in operational sea ice satellite monitoring, offering a good all-season capability (Onstott, 1992). With the launch of TerraSAR-X (2007) and COSMO Skymed (2007) new opportunities ~~in investigating~~ to investigate the potential use of X-band (frequency of 9,6 GHz) in sea ice satellite monitoring appeared. Several studies have investigated the application of X-band radar for sea ice mapping through ground based, airborne and satellite borne ~~plattforms~~platforms. X-band is found to have good separation capabilities between first-year ice and old ice (Onstott, 1992), between water and sea ice (Brath et al., 2013), and in detection of thin ice (Matsuoka et al., 2001). ~~For~~ Results from the Baltic Sea ~~, results show~~ suggest that the information content in C- and X-band are largely equivalent ~~(Mäkynen and Hallikainen, 2004; Eriksson et al., 2010).~~ (Mäkynen and Hallikainen, 2004; Eriksson et al., 2010), while X-band ~~has been~~ was found to add information when used in combination with C-band in the Arctic Ocean (Brath et al., 2013).

Several techniques for automatic segmentation of sea ice in SAR scenes exist. Methods consist of thresholding of polarimetric features, gamma distribution mixture models, K-means clustering, neural networks, Markov random field models, Gaussian mixture models, Wishart classifiers and iterative region growing using sematics (see Moen et al., 2013, and references therein). Several of these methods are feature-based methods, making use of a feature set in the segmentation. They have the advantage of being flexible as the input features used can be varied with, e.g., location and seasonal conditions, and the features offer possible post-segmentation information as an interpretation and labeling source. Moen et al. (2013) showed promising results in segmenting a full polarimetric sea ice scene taken under winter conditions (low temperatures and snow cover) with a simple feature-based multi-channel SAR segmentation method described in Doulgeris and Eltoft (2010) and Doulgeris (2013), utilising six polarimetric features ~~based on~~ derived from the covariance matrix.

Research has been conducted on SAR and microwave scatterometer measurements of sea ice since the early 1990s (Onstott, 1992). Most of the conducted studies have been in winter and late fall, and the number of studies in the melt period is limited. In winter, differences in salinity content and degree of deformation of sea ice make it possible to separate multi-year ice (MYI) and different stages of first year ice (FYI) from each other. During summer, more limited differences in salinity between MYI and FYI and the presence of moist snow ~~and free water~~ on the sea ice surface make monitoring with SAR challenging. SAR is sensitive to the large changes in relative permittivity connected to air temperatures close to zero degrees Celsius (Vant, 1974; Barber et al., 1998), and to variation in moisture content in the sea ice volume caused by freeze and thaw cycles (Scharien et al., 2010). Early studies on the use of SAR and microwave scatterometer data for summer sea ice applications can be found in, e.g., Onstott (1992); Gogineni et al. (1992); Carlstrom and Ulander (1993); Jeffries et al. (1997) and Yackel and Barber (2000). Newer studies include examination of backscatter signatures of multiyear sea ice with ship-based scatterometer (Isleifson et al., 2009) ~~,~~ and investigation of the use of a supplementary frequency of either X- or Ku-band in addition to C-band in late summer sea ice classification with an airborne scatterometer

(Brath et al., 2013), the possibility of separating . Satellite based studies include separation of MYI and FYI by dual polarisation intensity data from Radarsat-2 (Warner et al., 2013), classification potential of polarimetric features from Radarsat-2 (Gill et al., 2013) and investigations of melt pond fraction retrieval from co-polarisation ratio data acquired by Radarsat-2 (Scharien et al., 2012, 2014b). Separating different sea ice types during summer-melt is still a challenge.

The objective of this study is to investigate the potential of sea ice segmentation using C- and X-band multi-polarisation SAR features during late summer. A dataset consisting of five high resolution C- and X-band scenes recorded on iceberg-fast first-year and old ice in the Fram Strait in August and September 2011 is employed in our study. The satellite data is combined with airborne measurements from a helicopter flight at the site. We explore how the features and feature-based automatic segmentation successfully employed on FYI during winter conditions in Moen et al. (2013) perform on late summer sea ice with temperatures around the freezing point. Our study consists of two parts: firstly, the suitability of the individual features for use in late summer sea ice segmentation is evaluated. This is done by investigating the ability of the indicidual individual features to discriminate between sea ice types and their temporal consistency during changing temperature conditions. A reduced set of the four most temporally consistent features is suggested for use in segmentation. Secondly, a feature-based automatic segmentation algorithm is tested on the dataset. We investigate whether it groups the scenes into reasonable segments, possible to associate with distinct sea ice types. The algorithm is tested both with a full feature set, and with the reduced feature set suggested in the first part of the study. The segmented images are evaluated both visually, and by pixelvise evaluation of regions with known geophysical properties.

2 Methods

In this study, we examine the potential of six polarimetric SAR features for use in late summer sea ice segmentation. To simplify the study, five regions of interest (ROIs) with different

sea ice types ~~are~~ were defined based on information from the satellite scenes and the helicopter flight at the site. The first part of this section describes the dataset utilized in our study. In the second part we explain the design of the study, including the choice of ROIs, the generation of polarimetric SAR features and the ~~detailed~~ methodology of the analysis.

2.1 Study site

Fram Strait is a dynamic region characterised by the outflow of sea ice from the central Arctic Ocean (e.g. Kwok (2009b); Renner et al. (2014)). The sea ice cover is therefore highly variable with both FYI and MYI, and contains a large fraction of deformed ice. In late summer, the snow cover has usually melted completely, leading to melt ponds on top of the ice (e.g. Renner et al. (2013)). While in most parts of Fram Strait, southward drift leads to fast movement of the sea ice, a region with iceberg-fast ice forms in some years in western Fram Strait (Hughes et al., 2011). In this region, the ice cover varies between rough ice due to deformation and very level ice where the ice is formed during winter and protected from impact (Beckers et al., 2015; unpublished data). The study site was situated in this area (Fig. 1). Both FYI and old sea ice in different stages of development were represented at the site.

2.2 Dataset

The data used in this study were collected from ship, helicopter and satellite platforms during a coordinated campaign in the Fram Strait in late summer 2011. The dataset consists of several high resolution multi-polarimetric SAR scenes, together with airborne observations collected from a helicopter (Table 1). In addition, meteorological observations from the scientific vessel R/V *Lance* ~~are also available, offering~~ provided information about the changing weather conditions during the campaign. The area covered by the satellite scenes could not be reached by the ship, and the helicopter did not have the ~~oportunity~~ opportunity to land within the area, therefore no ~~ground based~~ in situ measurements from the sea ice surface were retrieved.

~~The study site is situated in an area with iceberg-fast sea ice located in the Fram Strait (see Fig. 1). Both first-year sea ice (FYI) and old sea ice in different stages of development are represented at the site.~~

2.2.1 Satellite measurements

For this study, three quad polarimetric C-band scenes from the Canadian Radarsat-2 (RS-2) satellite (denoted R1, R2 and R3) and two dual polarimetric X-band scenes from the German TerraSAR-X (TS-X) satellite (denoted T1 and T2) are used. More details about the scenes can be found in Table 1, and the ~~position~~ positions of the scenes are displayed in Fig. 1. All scenes ~~are recorded in~~ were acquired during ascending orbits. The RS-2 scenes have a coverage of 25 km (range) $\times$ 25 km (azimuth), while the TS-X scenes have a coverage of 15 km (range) $\times$ 50 km (azimuth).

2.2.2 ~~Air- and shipborne~~ Airborne measurements

Airborne measurements were conducted during a helicopter flight out from R/V *Lance* within the period of the satellite campaign (see Table 1). They include sea ice thickness, relative surface roughness and classified aerial images. The track of the flight is displayed together with the location of the satellite scenes in Fig. 1.

2.2.3 ~~Sea ice thickness~~

Measurements of total snow plus sea ice thickness (from now on referred to as sea ice thickness) were performed with an electromagnetic induction sounder (EM-bird), which was towed underneath the helicopter and flown at a height of about 15 m above the surface. More details about the EM-bird can be found in Haas et al. (2009); Renner et al. (2013, 2014). ~~In~~ From this device, the difference in conductivity between sea ice and water is used to find the height of the EM-bird above the ice/water interface, and a laser altimeter integrated in the EM-bird detects the distance between the EM-bird and the snow/ice surface. The difference between the two measures gives the sea ice thickness. The footprint of the

EM-bird has a diameter of about 50 m (depending on the height of the instrument). At the time of the acquisition there was very little or no snow on top of the sea ice, confirmed by the arial photos and observations from scientists onboard the helicopter.

2.2.3 ~~Surface roughness~~

The data from the laser altimeter mounted on the EM-bird can be used to extract surface roughness (von Saldern et al., 2006; Beckers et al., 2015). Calibration is needed to remove helicopter altitude variations. This was done by the three-step high- and low-pass filtering method described in Hibler (1972). The resulting surface elevation profiles are relative to the level ice. Surface roughness is in this study presented as the standard deviation of the profile surface elevation about the mean (root mean square height), R_q,

$$R_q = \sqrt{\frac{1}{N}\sum_{i=1}^{N}(y_i - \overline{y})^2}, \quad (1)$$

where N represents the number of measurements, $\overline{y}$ the mean height above level ice, and y_i the height above level ice of sample i. Each ROI profile is 400 m long, and N varies between 960 and 1067, depending on the speed of the helicopter.

2.2.3 ~~Melt pond fraction~~

The helicopter was equipped with a digital camera (GoPro YHDC5170, focal length 5 mm, view angle 127°), taking downward looking photographs of the sea ice surface. The area covered by each image was about 85 m (length) × 110 m (width) and the sampling rate was 0.5 Hz. The images were processed with a semi-automatic classification algorithm, separating classes of open water, submerged ice, melt ponds, very thin ice and thicker ice, as described in Pedersen et al. (2009) and Renner et al. (2013). In an accuracy assessment of the method performed in Renner et al. (2013), 76% of the melt pond pixels were correctly classified. The melt pond fraction, i.e., the percentage coverage of melt ponds retrieved

from each image, is used in our description of the sea ice types in this study. No additional ground information could be retrieved about the state of the melt ponds at the site of the satellite scenes during the campaign; hence we do not know whether the melt ponds were open or refrozen at the time of the acquisitions. According to the cruise report, open melt ponds were observed during the first days of the cruise, but from 26 August a major part of the melt ponds had started to freeze over. Melt pond measurements in open melt ponds at the ice edge were however performed until 31 August.

2.2.3 Meteorological information

SAR scattering properties of sea ice are highly affected by temperature and humidity, and meteorological information can therefore aid the interpretation of SAR satellite scenes. Meteorological measurements were performed on the scientific vessel R/V *Lance* during the campaign (Fig. 2). An automatic weather station at R/V Lance consisting of an air temperature sensor (3455), an air pressure sensor (2810) and a relative humidity sensor (3445), all from Aanderaa, were recording metorological information during the campaign (Fig. 2). The height of the station was 22 meters above sea level.S R/V *Lance* was sailing during this period and its route was located in the Fram Strait within 100 km west and north of the position of satellite scenes. During the week of data collection, the weather conditions were varying and the temperature was fluctuating around zero degrees Celsius. We have no recorded information about the amount of precipitation during the campaign, but the cruise report describes long periods with fog until 2 September. To investigate how the distance between R/V Lance and the position of the satellite scenes influenced the meteorological information, 2 meter air temperature and surface pressure were extracted from the European Center for Medium-Range Weather Forecastes (ECMWF) re-analysis (ERA-Interim) (Dee et al., 2011). The parameters were extracted in 6-hours increments for both the position of R/V Lance and the satellite scenes (79.25°N 14.25°W). There was good agreement between ERA-interim air temperature and surface pressure at the two locations (Fig. 2). The re-analysis seemed to overestimate the air temperature during the start of the campaign.

2.3 Study design

In the following subsections, the design of our study is presented.

2.3.1 Regions of interest

The area covered by the satellite scenes consists of sea ice with different geophysical properties. Some regions ~~are~~ were homogeneous and some ~~are~~ contained mixtures of different sea ice types. To simplify our study we focus on five different sea ice regions, representing the most typical sea ice types in the scenes (Fig. 3). The regions of interest (ROIs) ~~are~~ were chosen to be as homogeneous as possible, and to represent five distinctly different sea ice types. All ROIs are situated along the helicopter flight track and are 400 m (along track) $\times$ 200 m (across track) in size. The selection of the ROIs was performed manually, based on color coded polarimetric images (Pauli and composite-representations) of the satellite scenes together with photos, sea ice thickness, surface roughness and melt pond fraction retrieved from the helicopter overpass. Example photos from each ROI are presented in Fig. 4 and sea ice thickness histograms for each ROI can be found in Fig. 5. Table 2 presents helicopter measurements for each ROI, including mean and modal sea ice thickness, mean melt pond fraction, surface roughness, and sea ice class labels according to WMO sea ice nomenclature (World Meteorological Organisation, 1989). ROI1 ~~is representing~~ represents an area with level medium thick FYI, found in the upper left part of the scene in Fig. 3. The sea ice in ROI1 ~~is~~ was relatively smooth and ~~has~~ had a moderate melt pond fraction. ROI2 represents the area of level thin FYI located in the middle of the scene. The sea ice in ROI2 ~~is smooth with~~ was smooth with a high melt pond fraction. ROI3 and ROI4 ~~are both representing~~ represents areas of weathered deformed old ice, situated in the lower middle part of the scene. ROI3 represents thinner ice with a higher melt pond fraction than ROI4. ROI5 represents heavily deformed old ice, located in the lower part of the scene. Note that other areas of deformed ice can be seen as light-coloured regions in the right part of the scene possibly forming a shear ridge.

2.3.2 Polarimetric SAR features

Polarimetric SAR features combine information from the ~~different~~ channels of a multi-polarisation SAR system, and they represent information about the scattering properties of the surface. ~~This study investigates the sea ice discrimination and segmentation potential of six polarimetric SAR features during changing temperatures in late summer.~~ The features studied ~~are~~ were previously successfully used in segmentation of a winter time sea ice scene (Moen et al., 2013). An overview of the features and their definitions is presented in Table 3. The features consist of relative kurtosis (RK) geometric brightness (B), cross-polariation ratio ($R_{\mathrm{VH/VV}}$), co-polarisation ratio ($R_{\mathrm{VV/HH}}$), co-polarisation correlation magnitude ($|\rho|$) and co-polarisation correlation angle ($\angle\rho$). $R_{\mathrm{VH/VV}}$ is used instead of $R_{\mathrm{HV/HH}}$ as T2 has the polarisation combination VH $-$ VV. By inspection, these two features show similar values in our dataset. $\angle\rho$ is equivalent to the more frequently used term co-polarisation phase difference ($\phi_{\mathrm{HH-VV}}$).

A full-polarimetric SAR system is transmitting and receiving both horizontal (H) and vertical (V) polarised electromagnetic waves, resulting in $d = 4$ possible polarimetric channels (S_{HH}, S_{HV}, S_{VH} and S_{VV}). Assuming ~~reciproxivity~~ reciprocity ($S_{\mathrm{HV}} = S_{\mathrm{VH}}$), the Lexicographic feature vector, $\boldsymbol{s}$, is given by (Lee and Pottier, 2009)

$$\boldsymbol{s} = \begin{bmatrix} S_{\mathrm{HH}} & \sqrt{2}S_{\mathrm{VH}} & S_{\mathrm{VV}} \end{bmatrix}^{\mathsf{T}}, \tag{2}$$

where T denotes transpose. The covariance matrix, $\mathbf{C}$, is defined as the mean outer product of the Lexiographic feature vector (Lee and Pottier, 2009)

$$\mathbf{C} = \frac{1}{L}\sum_{i=1}^{L} \boldsymbol{s}_i \boldsymbol{s}_i^{*\mathsf{T}}, \tag{3}$$

where $\boldsymbol{s}_i$ is the single look complex vector corresponding to pixel i, L is the number of scattering vectors in a local neighbourhood and $*\mathsf{T}$ denotes the Hermitian transpose. Hence, $\mathbf{C}$

can be written as

$$\mathbf{C} = \begin{bmatrix} \langle S_{\mathrm{HH}} S_{\mathrm{HH}}^* \rangle & \langle S_{\mathrm{HH}} S_{\mathrm{VH}}^* \rangle & \langle S_{\mathrm{HH}} S_{\mathrm{VV}}^* \rangle \\ \langle S_{\mathrm{VH}} S_{\mathrm{HH}}^* \rangle & \langle S_{\mathrm{VH}} S_{\mathrm{VH}}^* \rangle & \langle S_{\mathrm{VH}} S_{\mathrm{VV}}^* \rangle \\ \langle S_{\mathrm{VV}} S_{\mathrm{HH}}^* \rangle & \langle S_{\mathrm{VV}} S_{\mathrm{VH}}^* \rangle & \langle S_{\mathrm{VV}} S_{\mathrm{VV}}^* \rangle \end{bmatrix}, \quad (4)$$

where the $\langle \cdot \rangle$ is the sample mean over L scattering vectors and * denotes the complex conjugate.

The TS-X scenes included in our study are ~~dual-plolarimetric~~dual-polarimetric. The covariance matrix then reduces to a 2×2 matrix. This implies that the full feature set of six features could not be achieved for these scenes since the achievable feature set depends on the scenes' polarimetric channel combination (see Table 3). Note that RK and ~~G~~ B in the TS-X scenes are calculated from reduced covariance matrices, and should not be directly compared to the similar RS-2 features.

$R_{\mathrm{VH/VV}}$, $R_{\mathrm{VV/HH}}$, $|\rho|$ and $\angle\rho$ are well known polarimetric features in sea ice applications (Drinkwater et al., 1992), while RK and B have seen less attention in the literature. RK is a measure of non-Gaussianity, and is defined as Mardia's multivariate kurtosis of a sample divided by the expected multivariate kurtosis of a complex normal distribution ($d(d+1)$) (Mardia, 1970; Doulgeris and Eltoft, 2010). RK < 1 points towards a distribution with broader shoulders and lighter tails than for Gaussian data, while RK > 1 implies a sharp peak close to the mean, and heavy tails relative to Gaussian distribution (DeCarlo, 1997). Large values of RK are expected for deformed sea ice due to scattering from a few strong reflections, and for inhomogeneous areas due to differences in intensity mixtures (Moen et al., 2013). B represents the intensity of the multichannel radar backscatter. It is closely related to the more familiar feature SPAN, i.e. trace($\mathbf{C}$), as they both represent the eignevalues of the covariance matrix. B is however more sensitive to the smaller eigenvalues. $R_{VH/VV}$ is known as a measure of depolarization (Drinkwater et al., 1992). In microwave scattering of sea ice, depolarization is expected related to multiple scattering within the sea ice volume or to surface roughness (Scharien et al., 2012; Moen et al., 2013). $R_{VV/HH}$ is only dependent on the relative permittivity for very smooth surfaces within the Brag regime (Hajnsek et al., 2003). For rougher surfaces, the feature is expected to increase

with incidence angle and relative permittivity, and decrease with increasing surface roughness (Drinkwater et al., 1991; Fung, 1994). With volume scattering, $R_{VV/HH}$ (dB) tends toward zero (Scharien et al., 2012). $|\rho|$ is a measure of the proportion of polarised backscatter, reaching unity when the co-polarisation channels are perfectly correlated (Drinkwater et al., 1992). The feature is expected to decrease with incidence angle, at an increasing rate for high salinity ice (Drinkwater et al., 1992; Gill et al., 2012). $\angle\rho$ is the relative difference in phase between the co-polarisation channels, describing the sea ice scattering history (Drinkwater et al., 1992). The feature depends on both the sea ice relative permittivity and surface roughness.

2.3.3 Data analysis

In the first part of our study, we examine the ability of the individual features to discriminate sea ice types, and their temporal consistency.

The sea ice type discrimination ability is evaluated through a maximum a posteriori (MAP) supervised classifier, using ~~Baye' s~~ Bayes' decision rule (Theodoridis and Koutroumbas, 2009). The classifier assigns pixel x to class ω_j if

$$P(\omega_j|x) > P(\omega_i|x) \quad \forall j \neq i. \tag{5}$$

where $P(\omega_j|x)$ is the probability of class ω_j given the feature value x. The probability density functions (~~pdfs) are~~ PDFs) were estimated with a Parzen kernel density estimator, using a Gaussian kernel function (Theodoridis and Koutroumbas, 2009). The bandwidth used is a function of the number of points in the sample and their distribution, as described in Bowman and Azzalini (1997). The pixels in the five ROIs were used as training areas, and each of the satellite scenes were classified inidvidually. As the ROIs investigated ~~are relatively small, hence~~ were small, resulting in small sample sizes, leave-one-out cross validation ~~is~~ was used in training and testing the classifier. A 7×7 pixels neighbourhood, $L = 49$, ~~is~~ was used in the classification and a stepping window with steps of 5×5 pixels was employed to reduce neighbourhood overlap. The resulting classification accuracies

obtained for each individual feature ~~are~~ were used to evaluate the discrimination abilities of the features in each of the five scenes.

The temporal consistency of the individual features is studied qualitatively for the three RS-2 scenes, by inspecting the mean ROI values of each feature. We consider a feature temporally consistent if the ranking of the mean ROI values of the feature are similar in all three scenes. E.g., the ROI with the highest mean value for a specific feature has the highest mean value of that feature in all the three investigated scenes. Based on the result on temporal consistency, a reduced feature set of four features is suggested.

In the second part of our study, a feature-based automatic segmentation algorithm is tested on the five scenes in the dataset. It is tested both with the original full feature set, and with a reduced feature set excluding the most temporally inconsistent features. The segmentation uses multivariate Gaussian mixture models to model the features' ~~pdf~~PDF, and employs an expectation-maximization algorithm. Markov random fields are used for contextual smoothing. Further description of the segmentation approach is given in Dougeris (2013) and Moen et al. (2013). A 21×21 pixels neighbourhood, $L = 441$, was used performing the segmentation. The large neighbourhood reduced the pixel resolution, but improved the results of the segmentation compared to a smaller neighbourhood, giving less granular segmentations. ~~A stepping window with steps of 5×5 pixels was used to reduce neighbourhood overlap, and an additional sub stepping window of 10×10 pixels was used during the algorithm for computation efficiency~~The size of the neigbourhood does not take into account the difference in resolution between the scenes, but assure an equal sample size in the extraction of the features. The algorithm was set to segment the scenes into six different ~~classes, to~~ segments. The number was chosen to allow for the five sea ice types described by the ROIs, in addition to one extra segment to allow for detection of ~~the major~~ other sea ice types ~~visually expected to be present in the scenes~~and to assure some flexibility for the algorithm. For easier comparison, the area used in the segmentation ~~is~~ was confined to the intersection of the individual scenes' geographical location (see the pink patch in Fig. ~~-~~1). For each scene, the segmentation's performance is evaluated visually ~~, and~~ on its ability to separate the four main sea ice types represented in the ROIs (medium

thick FYI, thin FYI, old ice and old deformed ice), and based on its ability to discriminate the pixels of the five ROIs into different ~~classes~~segments.

3 Results~~and discussion~~

This section ~~presents and discusses results from the two parts of our study. First, we~~ consists of three parts. The first two parts examine the individual sea ice type discrimination ability and the temporal consistency of six polarimetric SAR features~~during changing air temperature conditions. Secondly~~. In the third part, an automatic segmentation algorithm based on the investigated features is tested on the data set. Results for C- and X-band are presented separately, as differences in incidence angle, resolution and polarimetric channel combinations ~~makes~~ make a direct comparison inappropriate (see Table 1). The features in C-band are based on the full covariance matrix, while those in X-band are based on reduced covariance matrices as the TS-X scenes are dual polarisation scenes (see Table 3). Note that ROI5 is only present in the RS-2 scenes.

3.1 ~~Discrimination~~ Individual features discrimination ability~~and temporal consistency~~

In this section, we search for features that are suitable for use in late summer sea ice segmentation. We study both the ability of six individual features to discriminate sea ice types, and their temporal consistency during changing temperature conditions. Finally, we suggest a reduced feature set consisting on the four most temporally consistent features.

3.1.1 ~~Discrimination ability~~

~~The sea ice type classification accuracies recieved from the supervised MAP classification~~ The polarimetric features' individual capacity of classifying the investigated ROIs into separate classes are presented in ~~Tables~~ Table 4 and 5, for RS-2 and TS-X respectively. The presented values represent the diagonal values of the confusion matrices, i.e., the pre-

centage of true classfication. The best result for each ROI is highlighted in bold. All pixels from the five ROIs were included in the classification, and the experiment was performed separately for each of the scenes included in the study.

From the two tables we note that none of the features individually were able to classify all the five ROIs in a single scene with high accuracy. All features do however give satisfying classification results for some of the sea ice types represented by the ROIs, in some of the scenes. Hence, by combining the features, all features could add value to a feature-based sea ice type segmentation algorithm.

The best feature for discriminating a given ROI ~~is varying~~ varies from scene to scene. In all scenes except T1, ROI4 seems to be the most challenging to separate from the others. ROI4 ~~consist~~ consisted of old ice, as ~~does~~ did ROI3. An overlap between the ~~pdfs~~ PDFs of these two ROIs could be a reason for the poor discrimination result of ROI4.

In general, the result of the MAP classification for C- and X-band does not show large differences. The best classification accuracies in the C-band scenes are slightly higher than those in the X-band scenes, indicating a larger discrimination potential in C-band. This difference is not ~~nessecary~~ necessarily a result of different frequency. RK and B ~~is~~ are calculated from a reduced covariance matrix in the X-band scenes, and therefore contains less information. ~~Differences in incidence angle and resolution could also cause the lower accuracies in the X-band scenes~~The lower incidence angles of the TS-X scenes could also contribute to the observed differences.

3.1.1 ~~Temporal consistency~~

3.2 Temporal consistency of features

The temporal evolution of the ~~features' mean in each ROI is~~ feature means from each ROI are displayed in Figs. 6 and 7 for RS-2 and TS-X, respectively. The variances of the features within each ROI are displayed as error bars equivalent to two standard deviations. Due to different polarisation channel combinations (see Table 1), different features are displayed

for T1 and T2 in Fig. 7. This also limits a temporal investigation in X-band, and we will in the following focus on the results in C-band.

As weather conditions and incidence angles are different for the RS-2 scenes in the dataset (see Table1), the mean ROI values of the features ~~is~~ are expected to vary between the scenes even if sea ice conditions would be the same or very similar. Hence, when searching for ~~temporal~~ temporally consistent features, we look at the evolution of the ranking of the mean ROI values of each feature. For instance, studying RK in Fig. 6, the mean value within each ROI varies between the scenes. However, the relative relationship between the different mean values is almost constant. The RK of ROI5 does for instance take values between 1.05 and 1.15, but the RK value is always highest in this ROI. The same between-ROI-consistency during the investigated period can also be found for B, $R_{\mathrm{VH/VV}}$ and $\angle\rho$ (Fig. 6). The relative relationship of the mean ROI value of $R_{\mathrm{VV/HH}}$ and $|\rho|$ changes from scene to scene, hence no temporal consistency can be observed.

~~Sea ice relative permittivity is found to increase largely with increasing temperature as the sea ice temperature reaches above −7 to −5 °C (Vant, 1974; Barber et al., 1998). As the investigated scenes are all recorded at warm temperatures, a large variation in sea ice relative permittivity is expected between the scenes, even if the difference in air temperature between the scenes is relatively small. The temporal inconsistency of $R_{\mathrm{VV/HH}}$ and $|\rho|$ may indicate a stronger sensitivity to relative permittivity of these two features. In Bragg-scattering theory $R_{\mathrm{VV/HH}}$ is only dependent on the relative permittivity of the surface for a smooth surfaces (Fung, 1994). Based on differences in relative permittivity, FYI and old ice have been separated from saline young ice, leads and melt ponds by use of $R_{\mathrm{VV/HH}}$ (see Scharien et al., 2014a, and references therein).~~

~~Another possible reason for the inconsistency of these two features is a stronger sensitivity to changes in incidence angles than for the rest of the features. Note that the incidence angle of the three RS-2 scenes varies between 38 and 48(see Table 1). It is, however hard to reveal such a dependency from Fig. 6 for any of the features, indicating that the variation in mean ROI value of the features between the scenes is more dependent on~~

other conditions, for instance air temperature and moisture at the site, than on the incidence angle.

Gill et al. (2013) did a study on feature temporal consistency in C-band between a winter and a spring scene on FYI north of Canada. They found, similar to this study, that $\angle\rho$ showed high consistency during changing temperature conditions. In contradiction to our findings, they also found $R_{VV/HH}$ to have high temporal consistency. RK and B were not included in their study. The differences in results may be explained by different incidence angles, sea ice types and snow conditions.

T2 shows similar relationships between the mean ROI values of the features as the RS-2 scenes for all three features extracted (Figs. 6 and 7). The same between-ROI relationship can not be found for T1. This may be due to the air temperature being above zero degrees Celcius at the time of acquisition of this specific scene. The error bars in the TS-X ROIs are in general larger than in the RS-2 ROIs, which may indicate slightly poorer discrimination ability of the TS-X scenes.

3.2.1 Feature set for late summer sea ice segmentation

At the time of the campaign, the melt season was about to end. In this period with air temperatures fluctuating around the zero degrees Celcius, small changes in atmospheric conditions could have large impact on the sea ice surface properties. SAR is sensitive to the large changes in relative permittivity connected to air temperatures close to zero degrees Celsius (Vant, 1974; Barber et al., 1998), and to variation in moisture content in the sea ice volume caused by freeze and thaw cycles (Scharien et al., 2010).

A A feature-based sea ice segmentation algorithm for late summer sea ice is required is dependent on features with good discrimination ability and temporal consistency to give consistent results during changing atmospheric conditions, geophysical conditions. This is especially important as in situ information are often not availiable. Therefore, while searching for a suitable feature set for late summer sea ice segmentation, both the discrimination ability of the features and their temporally consistency are important. All features in our study showed some discrimination potential, but none could solely

discriminate between all ROIs in our study. Combining several of the features may improve the classification accuracy. Four out of the six investigated features were found to be temporally consistent in the period investigated. is often not available in the Arctic. Excluding temporally inconsistent features could help achieve a more temporally stable segmentation during changing atmospheric conditions. We therefore suggest a reduced feature set, consisting of RKRK, B, $R_{\mathrm{VH/VV}}$ $R_{VH/VV}$ and $\angle\rho$ for late summer sea ice segmentation. A reduction of features in the feature set could of course also imply loss of important information and hence degradation in the segmentation performance. The following section subsection will further explore the use of a reduced feature set.

3.3 Segmentation

In this section, the suitability of an automatic feature-based segmentation for late summer sea ice segmentation is tested. The segmentation is tested both with the full feature set including all six features investigated in this study (Table 3), and with a reduced feature set. The reduced feature set includes the features found to be the most temporally consistent in Sect. 3.2, hence $R_{\mathrm{VV/HH}}$ and $|\rho|$ are exluded. We evaluate the performance of the segmentation visually, and by its ability to discriminate the five ROIs from each other.

3.3.1 Segmentation performance

The segmented images for RS-2 are presented in Fig. 8, with the full feature set to the left and the reduced feature set to the right. The segmentations with the full feature set From Fig. 8, the segmentations of R1 (Fig. 8a) and R2 (Fig. 8c) both look reasonable compared to the information from the helicopter fligth. flight, both for the full (right) and reduced (left) feature set. The different segments seem to be associated with distinct sea ice types. One can recognise the thin FYI ice area in the middle of the scenes (violet), the heavily deformed old ice areas in the diagonal bottom-left part of the scenes (blue and turquoise), and two different sea ice classes north and south types north (medium thick FYI, orange) and south (old ice, yellow) of the middle regionwith thin FYI (orange and yellow). The segmentation

with the full feature set of R3 (Fig. 8e) has a more granular appearance. However, the thin FYI area in the middle (violet) and the heavily deformed old ice areas in the bottom-left diagonal part of the scene (blue and turquoise) are well segmented. The areas , and the areas with medium thick FYI north of the middle region, and the areas with old ice south of the middle region are confused are confused with the areas consisting of old ice (yellow, orange, grey). The differences between the segmentations with full and reduced feature sets for the three RS-2 scenes are in general small. The segmentation of R3 becomes slightly noiser noisier with the reduced feature set(Fig. 8). .

Figure 9 displays which classes segments the pixels of each of the ROIs are segmented were assigned to in all three RS-2 scenes, both for the full (left) and the reduced (right) feature sets. In general, the segmentations with the full feature set gives give good distinction between the different ROIs included in this study. In particular, the thin FYI in ROI2 and the deformed old ice in ROI5 are were separated with an accuracy above 71 % from the other ROIs in all of the three scenes. In R1 and R2 the segmentation is was not able to separate ROI3 and ROI4 clearly (Fig. 9a and c). These ROIs do both contain old ice, with different thicknesses and melt pond fractions, hence the ice types in the ROIs are quite similar. In R3 the medium thick FYI in ROI1 is misclassified between several classeswas segmented to three different segments. Reducing the feature set by exluding the temporally inconsistent features does not affect the results for R1 and R2 (Fig. 9b and d). In R3, it improves the separation of medium thick FYI in ROI1, and reduces the discrimination between the thin FYI in ROI2 and the old ice in ROI3 (Fig. 9f).

The segmentation segmentations of the two TS-X scenes, based on the achievable features limited by their polarisation channels (see Table 3), is are presented to the left in Fig. 10. In addition, T1 was segmented with a reduced feature set excluding co-polarisation ratio and co-polarisation correlation magnitude, presented to the right in the same figureFig. The segmentation of T1 with a full achievable feature set gives a poor and granular impression(see Fig. 10a). . The area of thin FYI in the middle of the scene is was not discriminated from the rest of the scene, and the deformed sea ice areas in the low left diagonal are were not fully segmented (sea green). The segmentation of T2 (Fig. 10c) also gives a slightly

granular impression, but the ~~larger segments~~ areas of thin FYI in the middle of the scene (violet)~~and deformed ice~~ , and the areas of deformed ice in the diagonal bottom-left part of the scene (blue and ~~turquise) are~~ turquoise) were well segmented. Reducing the feature set in the segmentation of T1 improves the segmentation of the area with thin first year ice in the middle of the scene (violet), even if granular noise is still present~~(orange) (Fig. 10b).~~ .

Figure 11 displays which ~~classes~~ segments the pixels in each of the ROIs ~~are segmented~~ were assigned to in the segmentation of the two TS-X scenes~~, for~~ . For T1 both for the full achievable (left) and the reduced (right) feature set. ~~Figure 11a confirms~~ Fig. 11a confirm the poor impression of the segmentation of T1 with full ~~acievable~~ achievable feature set, giving minimal discrimination between the four ROIs. In the segmented image of T2, the thin FYI in ROI2 can be separated from the other ROIs, but the rest of the ROIs ~~are~~ were mainly segmented into the same ~~class~~segment. Reducing the feature set in the segmentation of T1 (see Fig. 11b) does not improve the segmentation performance, even if the visual inspection of Fig. 10b gave a slight improvement for the whole scene.

3.3.1 ~~Segmentation evaluation~~

~~The tested automatic feature-based segmentation showed promising results for the RS-2 scenes, producing temporally consistent segmentations both for the full and~~

4 Discussion

Among the six investigated features, $R_{VV/HH}$ and $|\rho|$ were found temporal inconcistent during the study. The temporal inconcistency could have several reasons. These features might have a stronger sensitivity to sea ice relative permittivity than the others. As stated in the ~~reduced feature set. Reducing the feature set did only slightly degrade the segmentation performance in one of the scenes, hence $R_{VV/HH}$ and $|\rho|$ could be exluded from the feature set without a notable loss of information. The segmentation of R3 was somewhat more granluar than those of R1 and R2. The segmented~~ introduction, relative permittivity

will vary largely with temperature during warm conditions (Vant, 1974; Barber et al., 1998), and small temperature differences between the scenes could cause large differences in relative permittivity. In Bragg-scattering theory $R_{VV/HH}$ is only dependent on the relative permittivity of the surface for a smooth surfaces (Fung, 1994). Another possible reason for the inconsistency of these two features is a stronger sensitivity to changes in incidence angles than for the rest of the features. The incidence angle of the three RS-2 scenes ~~have different incidence angles and resolutions, and the meteorological conditions are different~~ varies between 38 and 48 degrees (see Table ~~1and Fig. 2). A drop in temperature and relative humidity prior to the acqisition of R3 could have caused rime on the sea ice surface (Drinkwater, 1995), or draining and refreezing of freshwater in the upper layers of the sea ice (Scharien et al., 2010). Both of which could cause a lower contrast between different sea ice~~ 1). $|\rho|$ varies linearly with incidence angle, according to Fig. 6, but the same dependency cannot be seen for $R_{VV/HH}$. Gill et al. (2013) did a study on feature temporal consistency in C-band between a winter and a spring scene on FYI north of Canada. They found, similar to this study, that $\angle\rho$ showed high consistency during changing temperature conditions. In contradiction to our findings, they also found $R_{VV/HH}$ to have high temporal consistency. RK and B were not included in their study. The differences in results may be explained by different incidence angles, sea ice types, ~~and hence hamper the segmentation result.~~ snow conditions and season.

~~The segmentation of the TS-X sceneswith the full achievable feature set showed poor performance for T1. In T2, some important regions were well segmented, even with only three achievable features out of the six used in~~ Choice of features and their temporal consistency is not the only factor affecting the results of the segmentation algorithm. Differences in incidence angle and resolution between the scenes, changing meteorological conditions and choice of segmentation parameters do all affect the outcome of our study. The incidence angles in our study vary between 26° (T2) and 48° (R2). As the backscatter signature from a sea ice surface depends on incidence angle, this is expected to affect the results. Between the RS-2 scenes, the incidence angle variation is small with a 10 °difference. From Fig. 6, it seems like the influence of the changing incidence angle is

limited, except for $|\rho|$. The pronounced difference in incidence angle between the RS-2 ~~scenes. Reducing the feature set slightly improved the segmentation performance of T1. The backscatter intensity (VV) in~~ and TS-X scenes could contribute to the poorer performance of the segmentation algorithm in X-band, but a larger number of scenes with overlapping incidence angle is needed to confirm this. To gain equal sample sizes in our study, the same neighbourhood size was used in filtering all scenes even if the scenes resolution differed. The scenes with highest resolution would therefore have smaller spatial filter sizes. This difference in scale possibly influences the signature of physical properties of the surface, like surface roughness variation. We did, however, during our investigations, also try to use filter sizes adjusted to the resolution, but this made little difference to the results.

During the week of data collection, the air temperature was varying around zero degrees Celsius, introducing difficult conditions for sea ice information retrieval from SAR. The distance between the meteorological measurements retrieved from R/V Lance and the study site makes detailed analysis of SAR weather dependence difficult. Some general meteorological events observed in the meteorological data could however help explain our results. Both T1 ~~is in general more than five dB lower than that in T2, but still well above the noise floor. According to the meteorological measurments from Lance, T1 was~~ and R2 were acquired during a ~~-~~period with air temperatures ~~above zero degree Celcius and high relative humidity (see Fig. 2). These conditions are probably at~~ close to or above zero degrees Celsius, conditions which is on the limit of ~~conditions~~ suitable for sea ice type discrimination by SAR. As reported by Scharien et al. (2010), moisture in the upper sea ice layer could mask out volume scattering ~~,~~and hence lower the backscatter contrast between different sea ice types. The ~~meteorlogical~~ difficult conditions could explain the poor segmentation performance of T1. ~~The improved segmentation of T1 with the reduced feature set could imply that the algorithm benefits from excluding temporally inconsistent features at air temperatures above zero degree Celcius~~

~~The poorer segmentation performance of the TS-X scenes, compared to the RS-2 scenes, is not necessarily a result of difference in frequency. Fewer polarisation channels,~~

~~lower incidence angles, different resolution and different geophysical conditions at the time of the aquisition could all contribute to a poorer segmentation~~ However, R2 was acquired during similar meteorological conditions with good segmentation results. Lower frequency, higher incidence angle and extra information contained in the cross-pol channel (lacking for T1) could all have contributed to a better segmentation of R2. The segmentation of R3 was poorer than those of the two other RS-2 scenes. Prior to the acquisition of R3, a drop in temperature and relative humidity could have caused rime on the sea ice surface (Drinkwater, 1995) or draining and refreezing of freshwater in the upper layers of the sea ice (Scharien et al., 2010). Both of which could cause a lower contrast between different sea ice types, and hence hamper the segmentation results. A refreeze of the sea ice could however also possibly result in the opposite, enhanced volume scattering could lead to increased sea ice type discrimination. ~~More scenes are required to investigate the limitations of the segmentation algorithm with respect to the above mentioned factors.~~

Choice of sliding window size and number of ~~classes~~ segments are important for the segmentation results. The use of window size of 21×21 pixels or larger showed the best results in our dataset. The size of the window was in our case a ~~-~~trade-off between resolution details (small window) and segmentation with little speckle and larger ~~continous~~ continuous regions (large window). The ~~number of classes~~ choice of window size will also determine which kind of information one retrieve about the sea ice surface. If information about small-scale structure like ridges, melt ponds and small leads are important, this requires a small window. For more general information for instance about sea ice age, larger window sizes could be more appropriate. Choice of sensor would set restrictions on how high resolution it is possible to achieve, and high resolution is at the moment coupled to small swath width. The number of segments was set in advance, based on visual inspection of the scenes and ~~in situ information~~ information retrieved from the helicopter-borne measurements. Choosing too few ~~classes~~ segments could force different sea ice types into a ~~common class~~common segment, while increasing the number of ~~classes~~ segments could split an ice type into several ~~classes~~segments.

5 Conclusions

This study examined the potential of sea ice segmentation by C- and X-band multi-polarisation SAR features during late summer in the Fram Strait. Firstly, the individual features sea ice type discrimination ability and their temporal consistency were investigated. Secondly, an automatic feature-based segmentation was tested.

The ability of the individual features to discriminate five sea ice types during changing temperature conditions was evaluated by a MAP supervised classifier, and by a qualitative study of the temporal consistency of the features. The classification results revealed a potential in all individual features for discriminating some of the sea ice types from each other, but none of the individual features could separate the total set of sea ice types in any of the scenes. Hence, a combination of the features has the potential of segmenting the different sea ice types included in our study. Temporal consistency was evaluated by studing the ability of the features to rank the mean value of the five sea ice types in the same order through the three RS-2 scenes. Relative kurtosis, geometric brightness, cross-polarisation ratio and co-polarisation correlation angle were found to give good temporal consistency during changing temperature conditions. These features were suggested as a reduced feature set. Co-polarisation ratio and co-polarisation correlation magnitude were found to be inconsistent through the period investigated. ~~A possible reason~~ Possible reasons for the two features inconsistency could be a ~~-~~higher sensitivity to changes in relative permittivity or incidence angles. Our study demonstrates some of the difficulties of sea ice type discrimination at temperatures close to zero degree Celcius, and highlights that it is important to cautiously select features for consistent sea ice monitoring during late summer. Our study shows as well that it is possible to retrieve valuable information from multi-polarisation SAR imagery, even under these difficult conditions.

An automatic feature-based segmentation algorithm was tested on the dataset and evaluated ~~visually and through~~ for its ability to discriminate the five investigated sea ice types. The segmentation was tested for a full feature set of six features and for a reduced feature set of the four features showing best temporal consistency. The segmentation ~~was in~~

~~general performing~~ in general performed well on the three RS-2 scenes. It showed good temporal consistency between the scenes, both for the full and for the reduced feature set. However, reducing the feature set did slightly degrade the sementation performance of one of the scenes. The segmentation succeeded in segmenting some of the sea ice types in one of the two TS-X scenes. In the other scene the segmentation performed poorly~~, probably due to~~ . The poor performance might be a result of air temperatures above ~~freezing point and hence difficult conditions for sea ice characterization by SAR~~zero degrees Celsius combined with low incidence angle and polarimetric channel combination (HH-VV). Reducing the feature set introduced a slight improvement in this poorest segmented scene. In total, the automatic feature-based segmentation algorithm demonstrates a potential of sea ice type discrimination during late summer, and our results indicate that an exclusion of ~~temporal~~ temporally inconsistent features could improve the segmentation results ~~when the temperature is close to or above freezing point~~in some cases. To confirm this, more scenes need to be investigated.

Both C- and X-band scenes were included in the study, but differences in incidence angles, resolution and number of polarisation channels made a direct comparison with respect to frequency inappropriate. One of the X-band scenes showed promising results when it came to sea ice type discrimination, close to those achieved for the quad polarimetric RS-2 scenes, even if it was a dual polarimetric scene. However investigations of more scenes with different incidence angle and polarisation combinations are necessary to reveal the potential of X-band in sea ice discrimination.

Future studies should also focus on a better physical understanding of the relation between SAR polarimetric features and geophysical properties~~which would be important for sea ice analysts to~~ . This could improve the interpretation ~~and labeling of~~ of the segmented sea ice scenes, and possibly lead to an automatically labeling the segments, a classification. The suitability of other features in late summer sea ice segmentation should also be explored. Multi-polarisation SAR images offer good possibilities for sea ice segmentation, but due to their limited swath width they are not suitable for operational ice charting. The development of compact polarimetry modes on new satellite missions like,

e.g, RISAT-1, PALSAR-2, and Radarsat Constellation Mission, and the new wide quad polarimetric mode in RS-2, could increase the amount of polarimetric information on larger swath widths, and the possibilities of late summer sea ice investigations in these modes should be investigated.

Acknowledgements. The authors would like to thank the captain, crew and scientist from the Norwegian Polar Institute onboard R/V *Lance* in the Framstrait 2011 for data collection. Thanks also to Justin Beckers at University of Alberta, Canada, for preprocessing the laser altimeter measurements. Radarsat-2 data are provided by NSC/KSAT under the Norwegian–Canadian Radarsat agreement 2011 and TerraSAR-X data are provided by InfoTerra. This project was supported financially by the project "Sea Ice in the Arctic Ocean, Technology and Systems of Agreements" ("Polhavet", subproject "CASPER") of the Fram Centre, and by the Centre for Ice, Climate and Ecosystems at the Norwegian Polar Institute. This project was also funded financially by Regional Differensiert Arbeidsgiveravgift (RDA) Troms County.

References

Barber, D. G., Yackel, J. J., Wolf, R. L., and Lumsden, W.: Estimating the thermodynamic state of snow covered sea ice using time series Synthetic Aperture Radar (SAR) data, in: International Society of Offshore and Polar Engineers Vol. III, The Eighth International Offshore and Polar Engineering Conference, 24–29 May 1998, Montreal, Canada, 50-541998.

Beckers, J. F., Renner, A. H., Spreen, G., Gerland, S., and Haas, C.: Sea-ice surface roughness estimates from airborne laser scanner and laser altimeter observations in Fram Strait and north of Svalbard, Ann. Glaciol., 56, 235–244, doi:10.3189/2015AoG69A717, 2015.

Bowman, A. W. and Azzalini, A.: Applied Smoothing Techniques for Data Analysis, Oxford University Press, New York, 1997.

Brath, M., Kern, S., and Stammer, D.: Sea ice classification during freeze-up conditions with multi-frequency scatterometer data, IEEE T. Geosci. Remote, 51, 3336–3353, 2013.

Carlstrom, A. and Ulander, L.: C-band backscatter signatures of old sea ice in the central Arctic during freeze-up, IEEE T. Geosci. Remote, 31, 819–829, doi:10.1109/36.239904, 1993.

Dabboor, M. and Geldsetzer, T.: Towards sea ice classification using simulated RADARSAT Constellation Mission compact polarimetric SAR imagery, Remote Sens. Environ., 140, 189–195, doi:10.1016/j.rse.2013.08.035, 2014.

DeCarlo, L. T.: On the meaning and use of kurtosis, Psychol. Methods, 2, 292–307, doi:10.1037/1082-989X.2.3.292, 1997.

Dee, D. P.,Uppala, S. M., Simmons, A. J., Berrisford, P., Poli, P., Kobayashi, S., Andrae, U., Balmaseda, M. A., Balsamo, G., Bauer, P., Bechtold, P., Beljaars, A. C. M., van de Berg, L., Bidlot, J., Bormann, N., Delsol, C., Dragani, R., Fuentes, M., Geer, A. J., Haimberger, L., Healy, S. B., Hersbach, H., Hólm, E. V., Isaksen, L., Kållberg, P., Köhler, M., Matricardi, M., Mcnally, A. P., Monge-Sanz, B. M., Morcrette, J. J., Park, B. K., Peubey, C., de Rosnay, P., Tavolato, C., Thépaut, J. N., and Vitart, F.: The ERA-Interim reanalysis: Configuration and performance of the data assimilation system, Quarterly J. Royal Meteorological Society,137,553-597, doi:10.1002/qj.828, 2011.

Doulgeris, A. P.: A simple and extendable segmentation method for multi-polarsation SAR images, in: Proc. of PolInSAR 2013, 6th International Workshop on Science and Applications of SAR Polarimetry and Polarimetric Interferometry, 28 January–1 February 2013, Frascati, Italy, ESA SP-713, European Space Agency, Paris, 2013.

Doulgeris, A. P. and Eltoft, T.: Scale mixture of Gaussian modelling of polarimetric SAR data, EURASIP J. Adv. Sig. Pr., 2010, 1–13, doi:10.1155/2010/874592, 2010.

Drinkwater, M.: Airborne and satellite SAR investigations of sea–ice surface characteristics, in: Oceanographic Applications of Remote Sensing, CRC Press, Boca Raton, Florida, 339–357, 1995.

Drinkwater, M., Kwok, R., Rignot, E., Israelsson, H., Onstott, R. G., and Winebrenner, D. P.: Potential applications of polarimetry to the classification of sea ice, in: Microwave Remote Sensing of Sea Ice, edited by: Carsey, F. D., vol. 68, Geophysical Monograph Series, American Geophysical Union, Washington, DC, 419–430, doi:10.1029/GM068, 1992.

Drinkwater, M., Kwok, R., Winebrenner, D. P., and Rignot, E.: Multifrequency polarimetric synthetic aperture radar observations of sea ice, J. Geophys. Res., 96, 20679–20698, doi:10.1029/91JC01915, 1991.

Eriksson, L. E. B., Borena, K., Dierking, W., Berg, A., Santoro, M., Pemberton, P., Lindh, H., and Karlson, B.: Evaluation of new spaceborne SAR sensors for sea-ice monitoring in the Baltic Sea, Can. J. Remote Sens., 36, S56–S73, 2010.

Fung, A. K.: Microwave Scattering and Emission Models and their Applications, Artech House Inc., Norwood, MA, 1994.

Gill, J. P., and Yackel, J. J.: Evaluation of C-band SAR polarimetric parameters for discrimination of first-year sea ice types, Can. J. Remote Sens., 38, 306–323, doi:10.5589/m12-025, 2012.

Gill, J. P., Yackel, J. J., and Geldsetzer, T.: Analysis of consistency in first-year sea ice classification potential of C-band SAR polarimetric parameters, Can. J. Remote Sens., 39, 101–117, doi:10.5589/m13-016, 2013.

Gogineni, S. P., Moore, R. K., Grenfell, T. C., Barber, D. G., Digby, S., and Drinkwater, M.: The effects of freeze-up and melt processes on microwave signatures, in: Microwave Remote Sensing of Sea Ice, edited by: Carsey, F. D., vol. 68, American Geophysical Union, Washington, DC, 329–341, 1992.

Haas, C., Lobach, J., Hendricks, S., Rabenstein, L., and Pfaffling, A.: Helicopter-borne measurements of sea ice thickness, using a small and lightweight, digital EM system, J. Appl. Geophys., 67, 234–241, doi:10.1016/j.jappgeo.2008.05.005, 2009.

Hajnsek, I. and Pottier, E. and Cloude, S.R.: Inversion of surface parameters from polarimetric SAR, IEEE T. Geosci. Remote, 41, 727–744, doi:10.1109/TGRS.2003.810702, 2003.

Hibler, W. D.: Removal of aircraft altitude variation from laser profiles of the arctic ice pack, J. Geophys. Res., 77, 7190–7195, doi:10.1029/JC077i036p07190, 1972.

Hughes, N. E., Wilkinson, J. P., and Wadhams, P.: Multi-satellite sensor analysis of fast-ice development in the Norske Øer Ice Barrier, northeast Greenland, Ann. Glaciol., 52, 151–160, 2011, doi:10.3189/172756411795931633, 2011.

Isleifson, D., Langlois, A., Barber, D. G., and Shafai, L.: C-band scatterometer measurements of multiyear sea ice before fall freeze-up in the Canadian Arctic, IEEE T. Geosci. Remote, 47, 1651–1661, 2009.

Jeffries, M. O., Schwartz, K., and Li, S.: Arctic summer sea-ice SAR signatures, melt-season characteristics, and melt-pond fractions, Polar Rec., 33, 101–112, doi:10.1017/S003224740001442X, 1997.

Kwok, R., Cunningham, G. F., Wensnahan, M., Rigor, I., Zwally, H. J., and Yi, D.: Thinning and volume loss of the Arctic Ocean sea ice cover: 2003–2008, J. Geophys. Res., 114, C07005, doi:10.1029/2009JC005312, 2009.

Kwok, R.: Outflow of Arctic Ocean Sea Ice into the Greenland and Barents Seas: 1979-2007, J. Climate, 22, 2438–2457, doi:10.1175/2008JCLI2819.1, 2009.

Laxon, S. W., Giles, K. A., Ridout, A. L., Wingham, D. J., Willatt, R., Cullen, R., Kwok, R., Schweiger, A., Zhang, J., Haas, C., Hendricks, S., Krishfield, R., Kurtz, N., Farrell, S., and Davidson, M.: CryoSat-2 estimates of Arctic sea ice thickness and volume, Geophys. Res. Lett., 40, 732–737, doi:10.1002/grl.50193, 2013.

Lee, J. S. and Pottier, E.: Polarimetric radar imaging: from basics to applications, CRC Press, Boca Raton, Florida, 2009.

Mäkynen, M. and Hallikainen, M.: Investigation of C- and X-band backscattering signatures of Baltic Sea ice, Int. J. Remote Sens., 25, 37–41, doi:10.1080/01431160310001647697, 2004.

Mardia, K. V.: Measure of multivariate skewness and kurtosis with applications, Biometrica, 57, 519–530, 1970.

Matsuoka, T., Uratsuka, S., Satake, M., Kobayashi, T., Nadai, A., Umehara, T., Maeno, H., Wakabayashi, H., Nakamura, K., and Nishio, F.: CRL/NASDA airborne SAR (Pi-SAR) observations of sea ice in the Sea of Okhotsk, Ann. Glaciol., 33, 115–119, 2001.

Meier, W. N., Hovelsrud, G. K., van Oort, B. E., Key, J. R., Kovacs, K. M., Michel, C., Haas, C., Granskog, M. A., Gerland, S., Perovich, D. K., Makshtas, A., and Reist, J. D.: Arctic sea ice in transformation: a review of recent observed changes and impacts on biology and human activity, Rev. Geophys., 52, 185–217, doi:10.1002/2013RG000431, 2014.

Moen, M.-A. N., Doulgeris, A. P., Anfinsen, S. N., Renner, A. H. H., Hughes, N., Gerland, S., and Eltoft, T.: Comparison of feature based segmentation of full polarimetric SAR satellite sea ice images with manually drawn ice charts, The Cryosphere, 7, 1693–1705, doi:10.5194/tc-7-1693-2013, 2013.

Onstott, R. G.: SAR and scatterometer signatures of sea ice, in: Microwave Remote Sensing of Sea Ice, edited by: Carsey, F., vol. 68, American Geophysical Union, Washington, DC, 73–104, 1992.

Parkinson, C. L. and Comiso, J. C.: On the 2012 record low Arctic sea ice cover: combined impact of preconditioning and an August storm, Geophys. Res. Lett., 40, 1356–1361, doi:10.1002/grl.50349, 2013.

Pedersen, C. A., Hall, R., Gerland, S., Sivertsen, A., Svenøe, T., and Haas, C.: Combined airborne profiling over Fram Strait sea ice: fractional sea-ice types, albedo and thickness measurements, Cold Reg. Sci. Technol., 55, 23–32, doi:10.1016/j.coldregions.2008.08.004, 2009.

Raney, R. K.: Hybrid-polarity SAR architecture, IEEE T. Geosci. Remote, 45, 3397–3404, 2007.

Renner, A. H. H., Dumont, M., Beckers, J., Gerland, S., and Haas, C.: Improved characterisation of sea ice using simultaneous aerial photography and sea ice thickness measurements, Cold Reg. Sci. Technol., 92, 37–47, doi:10.1016/j.coldregions.2013.03.009, 2013.

Renner, A. H. H., Gerland, S., Haas, C., Spreen, G., Beckers, J. F., Hansen, E., Nicolaus, M., and Goodwin, H.: Evidence of Arctic sea ice thinning from direct observations, Geophys. Res. Lett., 2012, 1–8, doi:10.1002/2014GL060369, 2014.

Scharien, R. K., Geldsetzer, T., Barber, D. G., Yackel, J. J., and Langlois, A.: Physical, dielectric, and C band microwave scattering properties of first-year sea ice during advanced melt, J. Geophys. Res., 115, C12026, doi:10.1029/2010JC006257, 2010.

Scharien, R. K., Yackel, J. J., Barber, D. G., Asplin, M., Gupta, M., and Isleifson, D.: Geophysical controls on C band polarimetric backscatter from melt pond covered Arctic first-year sea ice: Assessment using high-resolution scatterometry, J. Geophys. Res., 117, C00G18, doi:10.1029/2011JC007353, 2012.

Scharien, R. K., Landy, J., and Barber, D. G.: First-year sea ice melt pond fraction estimation from dual-polarisation C-band SAR – Part 1: In situ observations, The Cryosphere, 8, 2147–2162, doi:10.5194/tc-8-2147-2014, 2014a.

Scharien, R. K., Hochheim, K., Landy, J., and Barber, D. G.: First-year sea ice melt pond fraction estimation from dual-polarisation C-band SAR – Part 2: Scaling in situ to Radarsat-2, The Cryosphere, 8, 2163–2176, doi:10.5194/tc-8-2163-2014, 2014b.

Stephenson, S. R., Smith, L. C., Brigham, L. W., and Agnew, J. A.: Projected 21st-century changes to Arctic marine access, Climatic Change, 118, 885–899, doi:10.1007/s10584-012-0685-0, 2013.

Stroeve, J. C., Markus, T., Boisvert, L., Miller, J., and Barrett, A.: Changes in Arctic melt season and implications for sea ice loss, Geophys. Res. Lett., 41, 1216–1225, doi:10.1002/2013GL058951, 2014.

Theodoridis, S. and Koutroumbas, K.: Pattern Recognition, Academic Press, London, 2009.

Vant, M. R.: Dielectric properties of fresh and sea ice at 10 and 35 GHz, J. Appl. Phys., 45, 4712, doi:10.1063/1.1663123, 1974.

von Saldern, C., Haas, C., and Dierking, W.: Parameterization of Arctic sea-ice surface roughness for application in ice type classification, Ann. Glaciol., 44, 224–230, 2006.

Warner, K., Iacozza, J., Scharien, R., and Barber, D.: On the classification of melt season first-year and multi-year sea ice in the Beaufort Sea using Radarsat-2 data, Int. J. Remote Sens., 34, 3760–3774, doi:10.1080/01431161.2012.760855, 2013.

World Meteorological Organisation: Sea-ice nomenclature and interational system of sea ice symbols, Tech. rep., World Meteorological Organisation, Geneva, Switzerland, 1989.

Yackel, J. J. and Barber, D. G.: Melt ponds on sea ice in the Canadian Archipelago: 2. On the use of RADARSAT-1 synthetic aperture radar for geophysical inversion, J. Geophys. Res., 105, 22061, doi:10.1029/2000JC900076, 2000.

Table 1. Overview of the data set.

Date	Time (UTC)	Scene ID	Satellite, mode and polarisation	Incidence angle (°)	Pixel spacing (m) (azimuth × slant range)
29 Aug 2011	17:41	R1	Radarsat-2, Fine Quad, HH,HV,VH,VV	38.2°	5.0 m × 5.0 m
30 Aug 2011	18:23	T1	TerraSAR-X, StripMap, HH,VV	29.4°	2.4 m × 1.9 m
31 Aug 2011	18:23	R2	Radarsat-2, Fine Quad, HH,HV,VH,VV	48.2°	4.7 m × 5.1 m
3 Sep 2011	14:09	–	Helicopter fligth	–	–
4 Sep 2011	18:07	R3	Radarsat-2, Fine Quad, HH,HV,VH,VV	44.4°	5.1 m × 6.8 m
5 Sep 2011	17:00	T2	TerraSAR-X, StripMap, VH,VV	25.9°	2.3 m × 2.1 m

Table 2. Detailed information about the regions of interest (ROIs) from helicopter-borne measurments and the corresponding sea ice class labels (WMO nomenclatura).

ROI ID	Mean (modal) sea ice thickness (m)	Mean melt pond fraction (%)	Surface roughness, R_q (m)	Sea ice class labels
ROI1	1.3 (1.2) m	17 %	0.098 m	Medium thick first year ice
ROI2	0.6 (0.6) m	38 %	0.062 m	Thin first year ice
ROI3	2.1 (2.0) m	26 %	0.231 m	Old ice
ROI4	3.7 (3.3) m	11 %	0.204 m	Old ice
ROI5	11.7 (8.9) m	3 %	0.575 m	Old ice

Table 3. Polarimetric SAR features included in the study.

Polarimetric feature	Definition	Extracted for scene
Relative kurtosis	$\mathrm{RK} = \frac{1}{L}\frac{1}{d(d+1)}\sum_{i=1}^{L}\left[\mathbf{s}_i^{*\mathsf{T}}\mathbf{C}^{-1}\mathbf{s}_i\right]^2$	All scenes
Geometric brightness	$B = \sqrt[d]{\det(\mathbf{C})}$	All scenes
Cross-polarisation ratio	$R_{\mathrm{VH/VV}} = \frac{\left\langle S_{\mathrm{VH}} S_{\mathrm{VH}}^* \right\rangle}{\left\langle S_{\mathrm{VV}} S_{\mathrm{VV}}^* \right\rangle}$	R1, R2, R3, T2
Co-polarisation ratio	$R_{\mathrm{VV/HH}} = \frac{\left\langle S_{\mathrm{VV}} S_{\mathrm{VV}}^* \right\rangle}{\left\langle S_{\mathrm{HH}} S_{\mathrm{HH}}^* \right\rangle}$	R1, R2, R3, T1
Co-polarisation correlation magnitude	$\lvert\rho\rvert = \left\lvert \frac{\left\langle S_{\mathrm{HH}} S_{\mathrm{VV}}^* \right\rangle}{\sqrt{\left\langle S_{\mathrm{HH}} S_{\mathrm{HH}}^* \right\rangle \left\langle S_{\mathrm{VV}} S_{\mathrm{VV}}^* \right\rangle}} \right\rvert$	R1, R2, R3, T1
Co-polarisation correlation angle	$\angle\rho = \angle\left(\left\langle S_{\mathrm{HH}} S_{\mathrm{VV}}^* \right\rangle\right)$	R1, R2, R3, T1

Table 4. Classification accuracy of individual polarimetric features in the three Radarsat-2 scenes derived from MAP classification. The best result for each ROI ~~and the best overall accuracy for~~ in each scene are highlighted in bold.

Scene ID	Feature	Sea ice type classification accuracy (%)				
		ROI1	ROI2	ROI3	ROI4	ROI5
R1	RK	5	22	42	0	64
	B	1	**69**	**71**	**10**	**78**
	$R_{\mathrm{VH/VV}}$	**23**	0	38	0	51
	$R_{\mathrm{VV/HH}}$	7	49	15	0	40
	$\lvert\rho\rvert$	0	41	31	5	46
	$\angle\rho$	0	30	70	0	41
R2	RK	41	28	0	7	8
	B	31	63	**75**	**32**	23
	$R_{\mathrm{VH/VV}}$	19	**87**	0	18	**44**
	$R_{\mathrm{VV/HH}}$	0	70	40	0	26
	$\lvert\rho\rvert$	**57**	0	0	0	34
	$\angle\rho$	5	11	19	27	**44**
R3	RK	0	20	**60**	40	55
	B	38	45	24	26	54
	$R_{\mathrm{VH/VV}}$	3	40	2	40	**74**
	$R_{\mathrm{VV/HH}}$	**61**	35	0	**41**	0
	$\lvert\rho\rvert$	31	**50**	6	2	58
	$\angle\rho$	14	0	0	23	51

Table 5. Classification accuracy of individual polarimetric features in the two TerraSAR-X scenes derived from MAP classification. The best result for each ROI in each scene is highlighted in bold.

Scene ID	Feature	Sea ice type classification accuracy (%)			
		ROI1	ROI2	ROI3	ROI4
T1	RK	35	3	**24**	17
	B	54	0	21	**60**
	$R_{\mathrm{VV/HH}}$	54	17	16	19
	$\lvert\rho\rvert$	51	**44**	0	19
	$\angle\rho$	**59**	12	22	18
T2	RK	**44**	0	32	6
	B	41	23	**59**	10
	$R_{\mathrm{VH/VV}}$	16	**61**	19	**23**

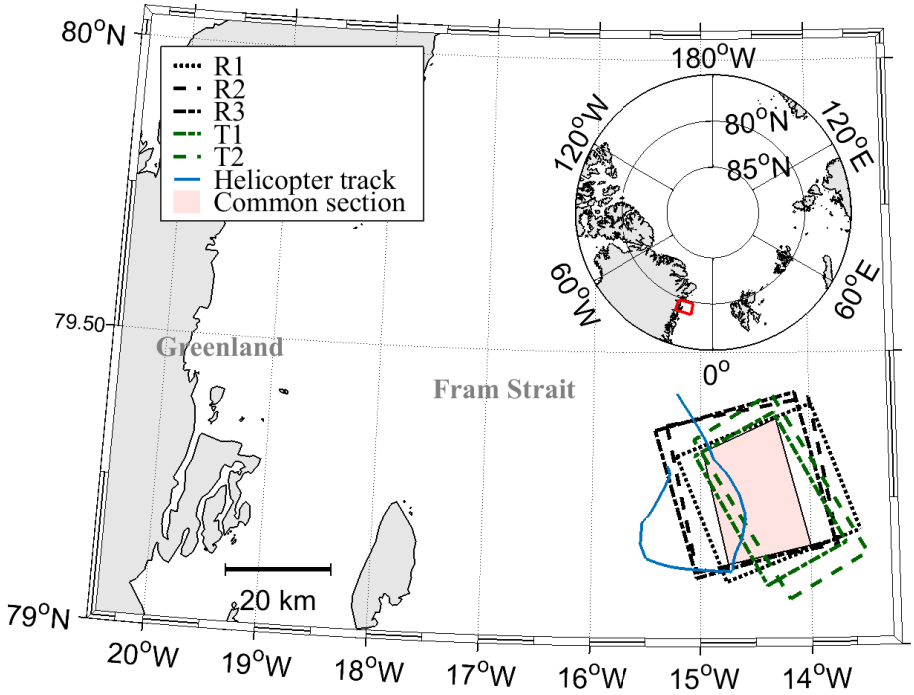

Figure 1. Map of the western Fram Strait showing the location of the satellite scenes included in the study and the track of the helicopter flight collecting airborne measurements for the study. The red box in the inset map of the Northern Hemisphere displays the geographical position of the area displayed. At the time of the flight, R/V *Lance* was slightly north of this map section.

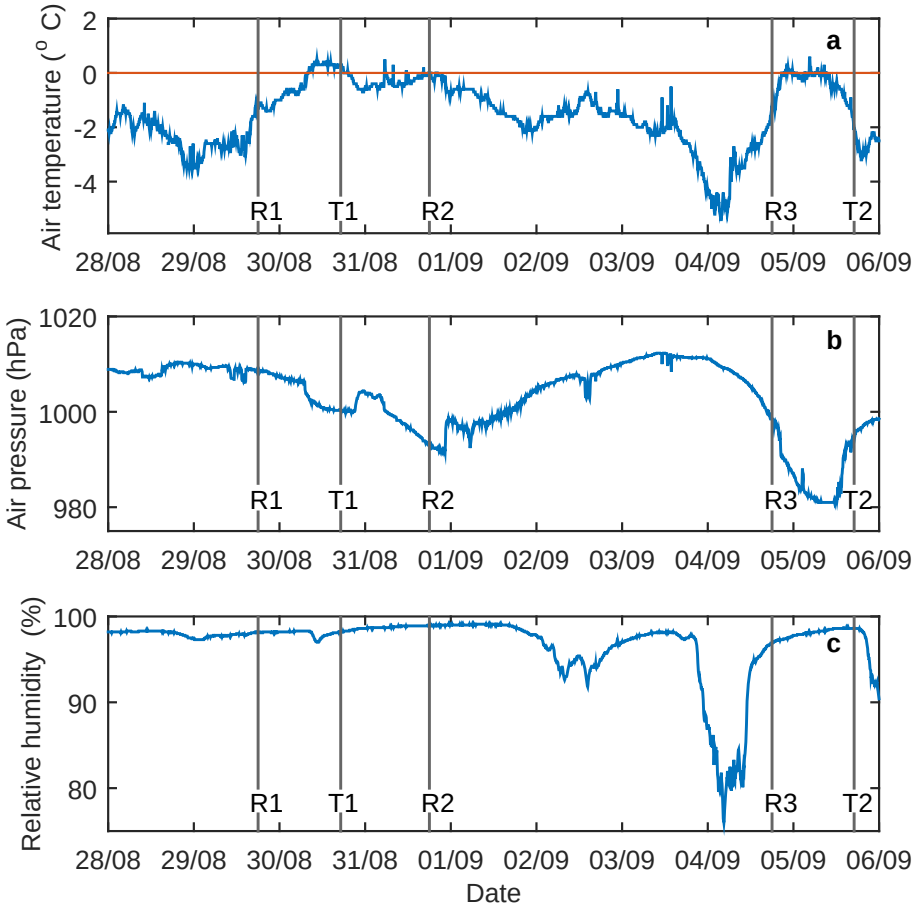

Figure 2. Air temperature **(a)**, air pressure **(b)** and relative humidity **(c)** during the campaign. The gray vertical lines represent the time of the acquisition of the satellite scenes.

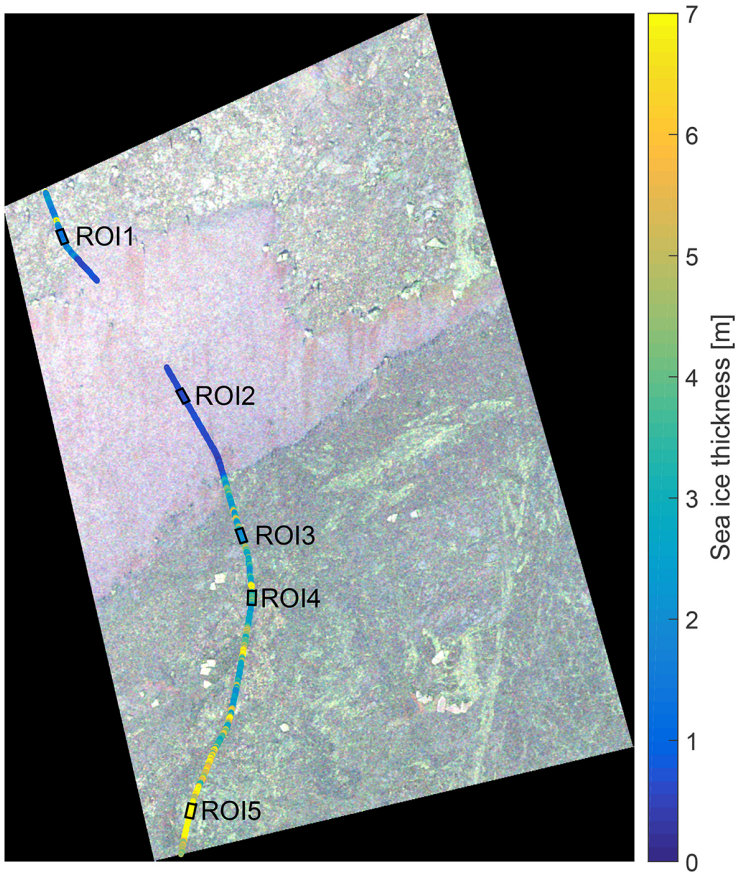

Figure 3. Position of regions of interest and helicopter thickness measurements displayed on the Radarsat-2 scene from 31 August 2011 (R2). The polarimetric image is a Pauli composite, the intensity channel combinations $|HH - VV|$, $2|HV|$ and $|HH + VV|$ are assigned to the red, green and blue (RGB) channels, respectivly.

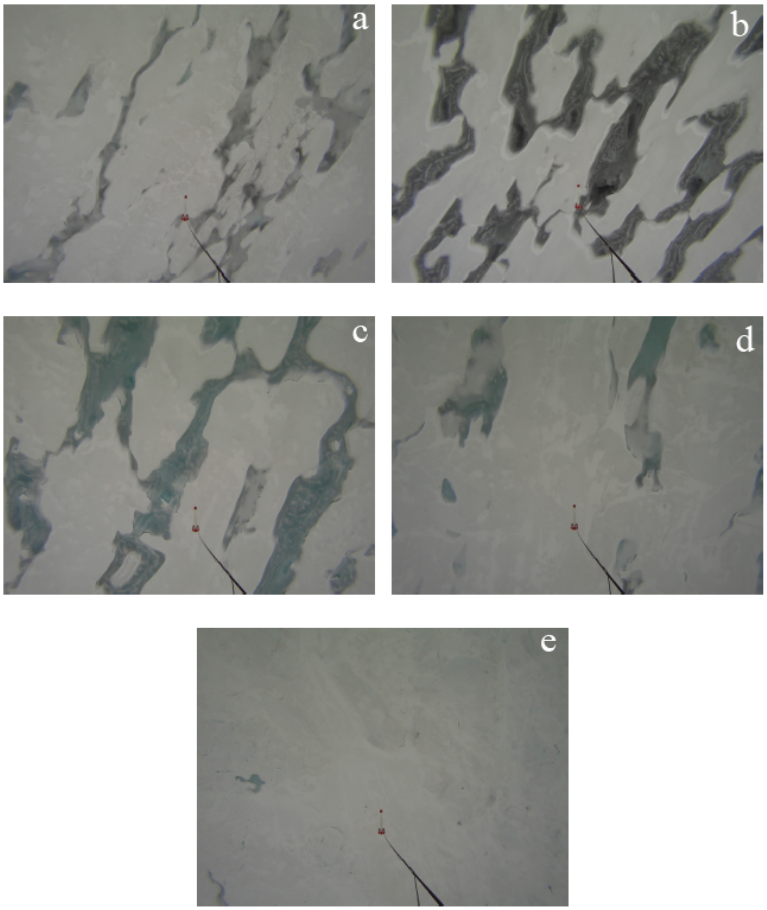

Figure 4. Example photos from the five regions of interest: **(a)** ROI1, **(b)** ROI2, **(c)** ROI3, **(d)** ROI4 and **(e)** ROI5. The photos are captured during the helicopter flight on 3 September 2011, and the EM-bird can be seen in the lower center part of each photo.

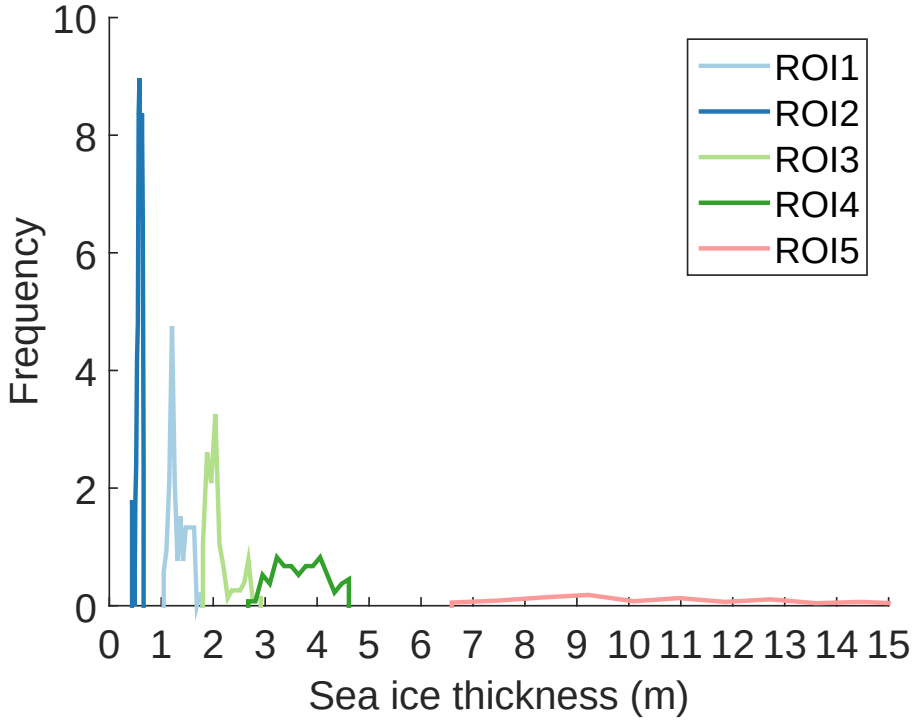

Figure 5. Histograms of sea ice thickness (m) measured during the helicopter flight 3 September 2011 for each of the five regions of interest.

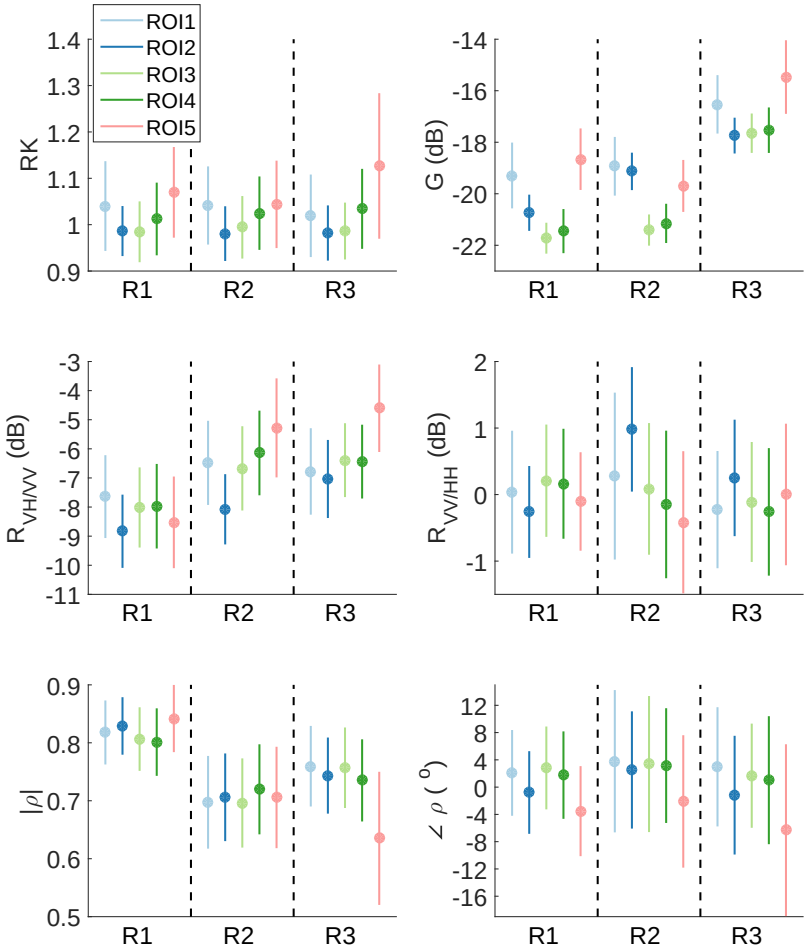

Figure 6. Mean values of the features in the regions of interest in the three Radarsat-2 scenes (R1, R2 and R3). The error bars are two standard deviations long.

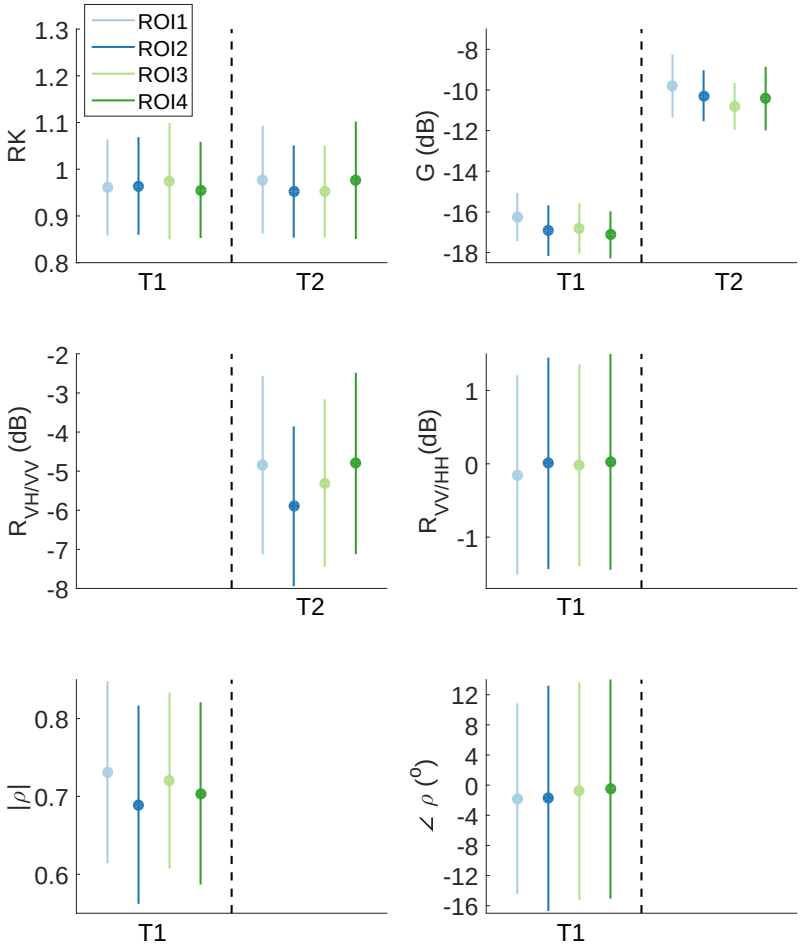

Figure 7. Mean values of the features in the regions of interest in the two TerraSAR-X scenes (T1 and T2). The error bars are two standard deviations long.

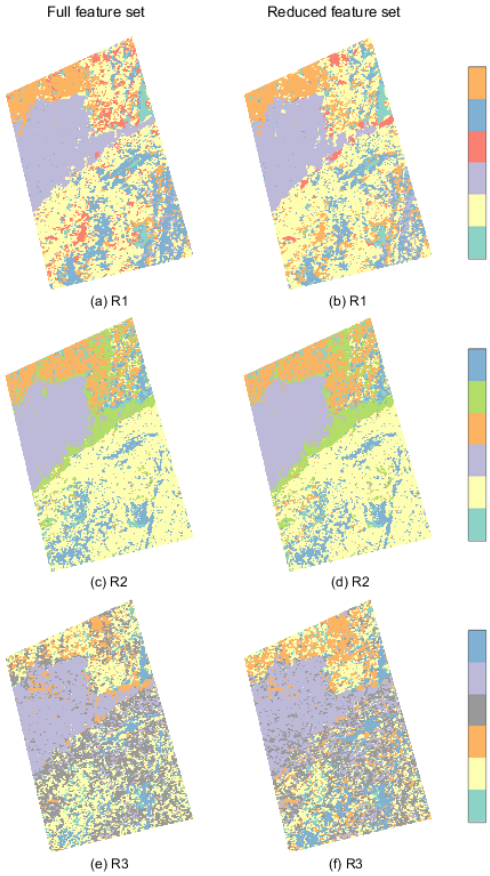

Figure 8. Segmentations of the three Radarsat-2 scenes (R1, R2 and R3) into six ~~classes~~segments. To the left: segmentation with full feature set. To the right: segmentation with reduced feature set consisting of relative kurtosis, geometric brightness, cross-polarisation ratio and co-polarisation angle.

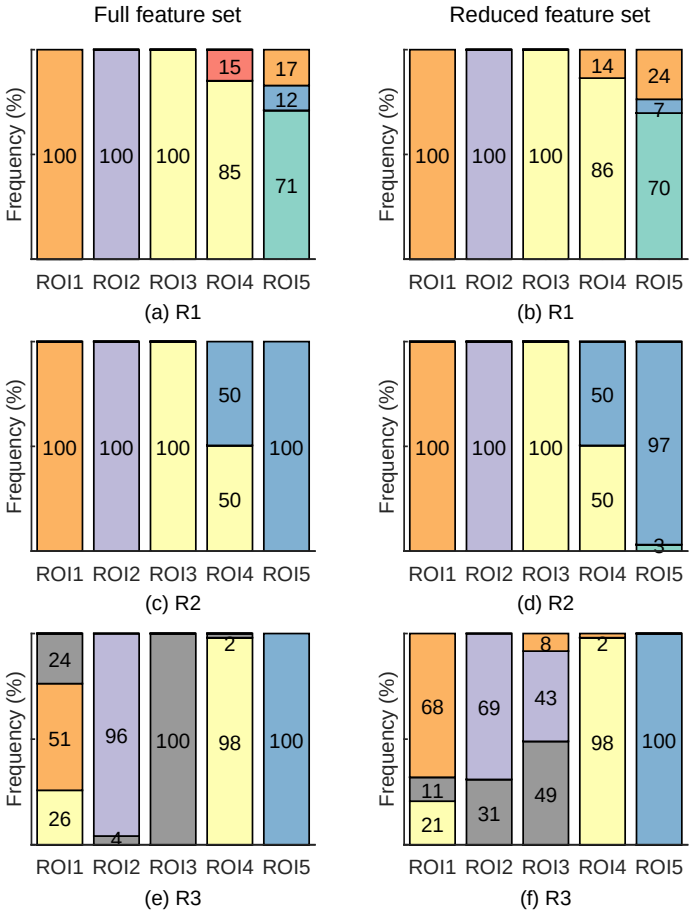

Figure 9. The ~~classes assinged~~ segments assigned to the pixels in the five regions of interest by the segmentation of the three Radarsat-2 scenes (R1, R2 and R3). To the left: segmentation with full feature set. To the right: segmentation with reduced feature set.

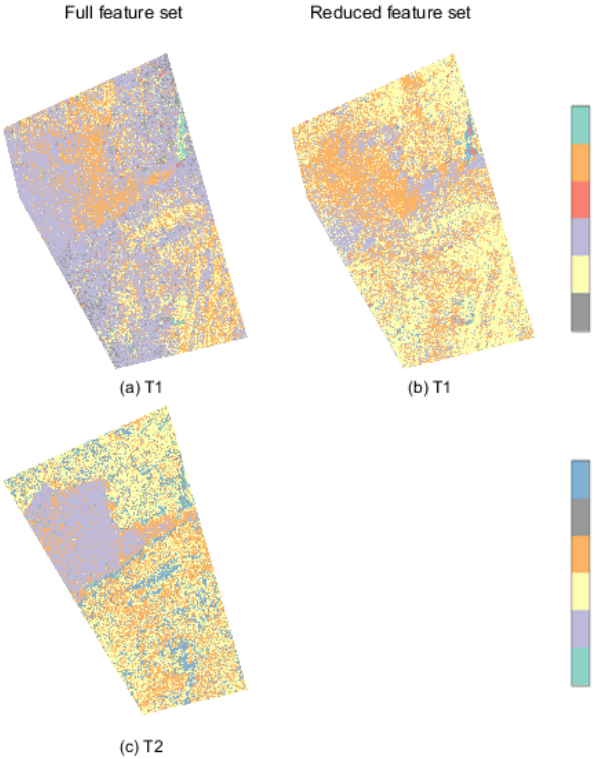

Figure 10. Segmentations of the two TerraSAR-X scenes (T1 and T2) into six ~~classes~~segments. To the left: segmentation with full achievable feature set. For T1 the feature set consists of relative kurtosis, geometric brightness, co-polarisation ratio, co-polarisation correlation magnitude and co-polarisation correlation angle. For T2 the feature set consists of relative kurtosis, geometric brightness and cross-polarisation ratio. To the right: segmentation of T1 with the reduced feature set consisting of relative kurtosis, geometric brightness and co-polarisation correlation angle.

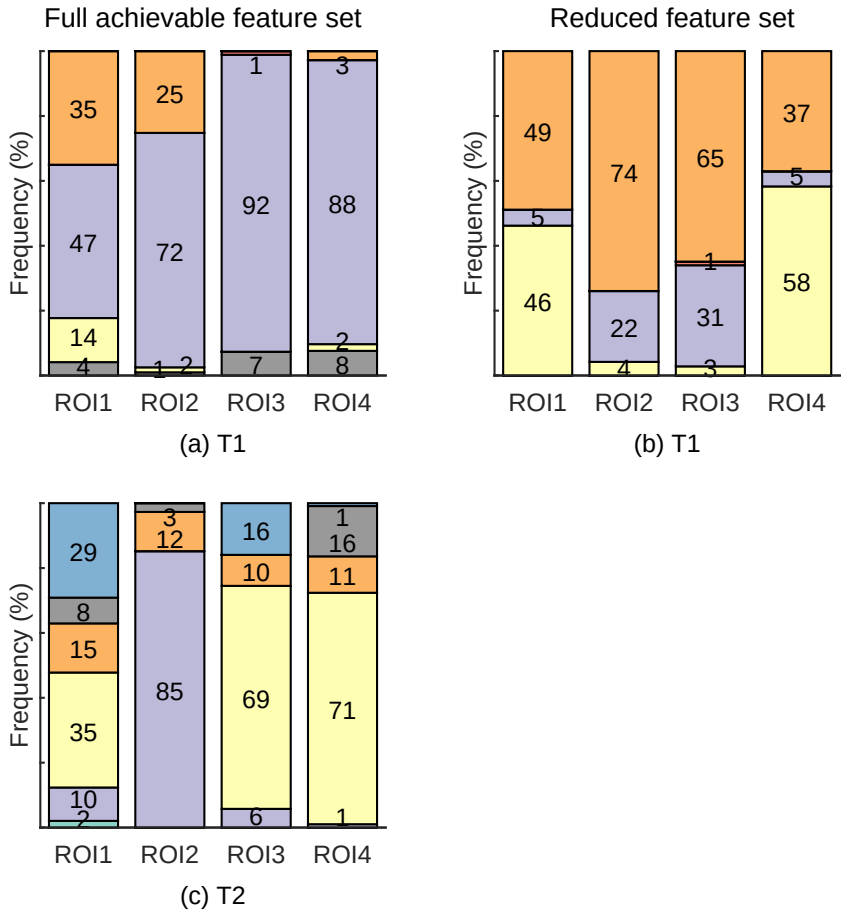

Figure 11. The ~~classes assinged~~ segments assigend to the pixels in the five regions of interest by the segmentation of the two TerraSAR-X scenes (T1 and T2). To the left: segmentation of T1 and T2 with full achievable feature set. To the right: segmentation of T1 with reduced feature set.